Moyamoya disease susceptibility gene RNF213 links inflammatory and angiogenic signals in endothelial cells

大久保，一宏

https://doi.org/10.15017/1560379

出版情報：九州大学，2015，博士（医学），課程博士
バージョン：

SCIENTIFIC REPORTS

OPEN

Moyamoya disease susceptibility gene *RNF213* links inflammatory and angiogenic signals in endothelial cells

Received: 19 March 2015
Accepted: 03 July 2015
Published: 17 August 2015

Kazuhiro Ohkubo[1,*], Yasunari Sakai[1,*], Hirosuke Inoue[1], Satoshi Akamine[1], Yoshito Ishizaki[1], Yuki Matsushita[1], Masafumi Sanefuji[1], Hiroyuki Torisu[1,3], Kenji Ihara[1,2], Marco Sardiello[4] & Toshiro Hara[1]

Moyamoya disease (MMD) is a cerebrovascular disorder characterized by occlusive lesions of the circle of Willis. To date, both environmental and genetic factors have been implicated for pathogenesis of MMD. Allelic variations in *RNF213* are known to confer the risk of MMD; however, functional roles of RNF213 remain to be largely elusive. We herein report that pro-inflammatory cytokines, IFNG and TNFA, synergistically activated transcription of *RNF213* both *in vitro* and *in vivo*. Using various chemical inhibitors, we found that AKT and PKR pathways contributed to the transcriptional activation of *RNF213*. Transcriptome-wide analysis and subsequent validation with quantitative PCR supported that endogenous expression of cell cycle-promoting genes were significantly decreased with knockdown of *RNF213* in cultured endothelial cells. Consistently, these cells showed less proliferative and less angiogenic profiles. Chemical inhibitors for AKT (LY294002) and PKR (C16) disrupted their angiogenic potentials, suggesting that RNF213 and its upstream pathways cooperatively organize the process of angiogenesis. Furthermore, RNF213 down-regulated expressions of matrix metalloproteases in endothelial cells, but not in fibroblasts or other cell types. Altogether, our data illustrate that RNF213 plays unique roles in endothelial cells for proper gene expressions in response to inflammatory signals from environments.

Moyamoya disease (MMD) represents a specific intracranial vascular disorder characterized by progressive, occlusive lesions of internal carotid arteries and branches in the circle of Willis[1,2]. To compensate the decreased blood flow in the affected brain area, the fine vascular network of *Moyamoya*, a Japanese word meaning "puffs of smoke", develops as arterial stenosis progress[1,2]. Earlier studies demonstrated that environmental factors including varicella zoster virus infection contributed to the development of MMD[3,4]. On the other hand, population-based studies pointed to the higher incidence of MMD in oriental populations than those in Caucasians, suggesting that certain genetic backgrounds may also confer the risk for the development of the vascular lesions[5].

Genetic studies for MMD patients have been conducted to identify candidate disease susceptibility loci[6–10]. Notably, several groups have demonstrated that single nucleotide variations in the *RNF213* gene had a strong association with the onset of MMD in both familial and sporadic cases[11,12]. The human

[1]Department of Pediatrics, Graduate School of Medical Sciences, Kyushu University, Fukuoka 812-8582, Japan. [2]Department of Pediatrics, Faculty of Medicine, Oita University, Yufu 879-5593, Japan. [3]Section of Pediatrics, Department of Medicine, Fukuoka Dental College, Fukuoka 814-0193, Japan. [4]Department of Molecular and Human Genetics, Baylor College of Medicine, Jan and Dan Duncan Neurological Research Institute, Texas Children's Hospital, Houston 77030, USA. *These authors contributed equally to this work. Correspondence and requests for materials should be addressed to Y.S. (email: ysakai22q13@gmail.com)

RNF213 gene encompasses a 137,922-bp region at chromosome 17q25.3 (chr17:78,234,660–78,372,581) and consists of 68 exons with 67 protein-coding exons. The encoded 596-kDa protein, RNF213, harbors AAA-type ATPase, alpha-2-macroglobulin, and ring finger domains from its amino to carboxyl terminus[13]. Because of the presence of ring finger domain(s), RNF213 is considered a member of E3 ubiquitin ligase protein family. Recently, RNF213 has been reported to be associated with angiogenesis[14]; however, little is known about its endogenous functions or its pathogenic roles in MMD[13,15].

To uncover the functional roles of RNF213 and pathogenic processes underlying MMD, we took advantage of bioinformatics approaches to analyze hundreds of transcriptomic data publicly available at open databases[16]. The bioinformatics data predicted that RNF213 might act cooperatively with other molecules under inflammatory signals. Based on this unbiased prediction, we investigated whether RNF213 might respond to pro-inflammatory stresses. Through a series of functional studies, we herein propose that RNF213 links the gap between environmental risk factors for the onset of MMD and endogenous signaling that is essential for angiogenesis.

Results

RNF213 is associated with immune response. We reasoned that identifying endogenous functions of RNF213 would facilitate our work towards unraveling the pathogenic mechanisms of MMD. To this end, we hypothesized that co-expression analysis can drive the prediction of functional pathways that RNF213 might regulate or be involved in. We took a bioinformatics approach to perform an unbiased analysis on the expression profile of *RNF213* in a large collection of human tissues and experimental conditions[16,17]. Gene Ontology (GO) analysis of the genes that showed highly correlated in expressions with *RNF213* was then performed to infer putative pathways where RNF213 might play a functional role (Supplementary Fig. S1 and Supplementary Table S1). We found that the GO categories of "immune response", "response to virus", "defense response", "inflammatory response", and "innate immune response" were significantly enriched and were consistently ranked at the top list of GO categories (Supplementary Fig. S1 and Supplementary Table S1). These data suggested that *RNF213* may be functionally associated with immune systems and/or virus defense. It was also noted that the GO term of "protein kinase cascade" was significantly enriched in the co-expression analysis. *RNF213* was therefore likely co-regulated with other genes under stressed conditions, such as inflammation or infections.

Pro-inflammatory cytokines activate the transcription of *RNF213*. Based on the bioinformatic prediction above, we next explored the exogenous ligands that may affect the endogenous expression of *RNF213* in cultured endothelial cells. We first stimulated HUVECs with various ligands for innate immunity or cytokines, including polyI:C, LPS, PMA/ionomycin, IFNA, IFNG, TNFA, TGFB, IL-1B, IL-2, IL-6, IL-18, and rapamycin[18]. We found that *RNF213* mRNA in HUVECs was significantly up-regulated when the cells were treated with IFNA or IFNG (Fig. 1a). Because TNFA was known to promote angiogenesis[19,20], we additionally examined *RNF213* mRNA level with co-stimulation of the cells with TNFA and IFNG. The result showed that TNFA and IFNG combination further enhanced the expression level of *RNF213*, supporting the synergistic effects of pro-inflammatory cytokines on endothelial gene responses (Fig. 1b). Similar results were also obtained in HCAECs (Supplementary Fig. S2). The stimulatory effect of IFNG on the expression of *RNF213* in endothelial cells was verified at the protein level (Fig. 1c). We also tested whether the genes that were predicted to be co-regulated with *RNF213* (Supplementary Table S1) were also up-regulated with such cytokine treatments. We randomly selected 15 genes (25.4%) from those listed in Supplementary Table S1, and appended *IL-6* as a positive control for the IFNG treatment[21]. We ensured that IL-6 expression was increased 1.6-fold to the basal level, and that all of the 15 genes were robustly induced by the IFNG treatment (Fig. 1d). We also verified that the increase of *RNF213* mRNA was the result of transcriptional activation, rather than increased stability of mRNA, because a low-dose treatment with the RNA polymerase inhibitor, actinomycin D (500 μg/ml), efficiently blocked the acute increase in the amount of *RNF213* transcripts upon cytokine stimulation (Fig. 1e). We therefore concluded that the expression of *RNF213* was up-regulated by pro-inflammatory cytokines in a transcription-dependent manner in cultured endothelial cells.

We then investigated the relevance of these data to physiological and stressed conditions *in vivo*. In wild-type, 4-week-old female mice (C57BL/6), *Rnf213* proved to be expressed in various tissues, including brain, heart, great vessels, mononuclear cells and spleen. We verified that the heart was the organ with the highest expression of *Rnf213* (Fig. 1f). When we treated these mice with an intra-peritoneal injection of murine IFNG and TNFA, the mRNA level of *Rnf213* was significantly elevated at 6 hr after injection and rapidly declined within 24 hr (Fig. 1g). Intriguingly, the IFNG and TNFA injection activated the expression of *Rnf213* most prominently in heart and great vessels among other tissues. Together, these results demonstrate that *RNF213* is activated by inflammatory signals from the environment both *in vitro* and *in vivo*.

AKT and PKR pathways up-regulate the transcription of *RNF213*. To identify the upstream pathway(s) that controlled the transcriptional activation of *RNF213* in response to cytokines, we treated HUVECs with various protein kinase inhibitors. These included LY294002 for PI3K-AKT, C16 for PKR, U0126 monoethanolate for MEK-ERK, AG490 for JAK-STAT, and SP600125 for JNK[22,23]. Among them, LY294002 and C16 significantly suppressed the transcriptional activation of *RNF213* in endothelial cells

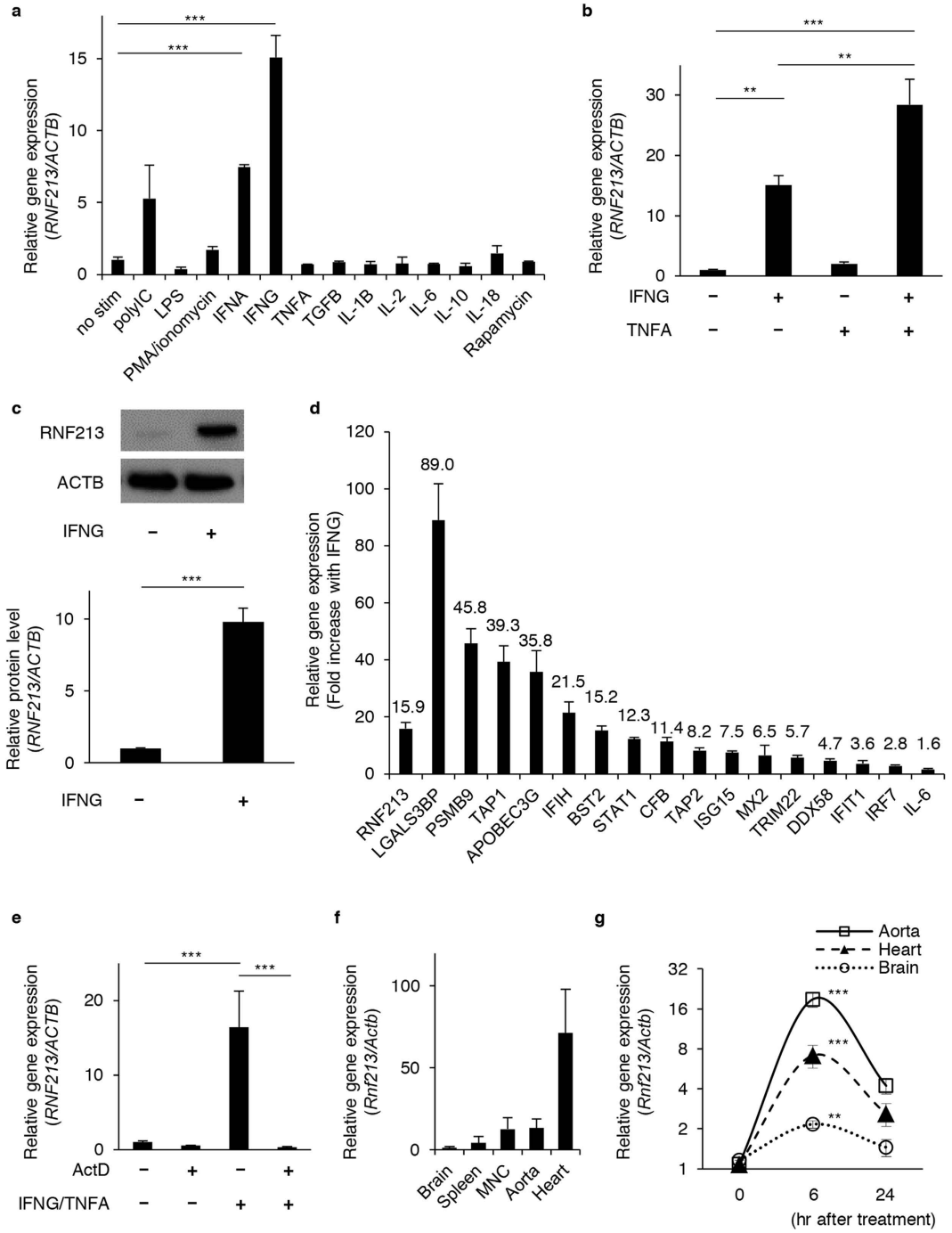

Figure 1. *RNF213* is transcriptionally activated by IFNG and TNFA *in vitro* and *in vivo*. (**a**) Relative expressions of *RNF213* in HUVECs when stimulated with various ligands for innate immunity and cytokines in comparison to that of control ("No Stim"). (**b**) Synergistic effects of IFNG and TNFA treatments on *RNF213* expression in HUVECs. (**c**) Western blot analysis for the RNF213 protein induction with IFNG treatments in HUVECs. Quantified results are plotted under the blotting image. (**d**) Coinstantaneous inductions of *RNF213* and other co-expressed genes upon IFNG treatments of HUVECs. (**e**) Suppression of *RNF213* induction after IFNG and TNFA treatments by actinomycin D (ActD) for HUVECs. (**f**) The steady-state *Rnf213* expressions in various tissues of female mice at 4-weeks of age (compared with Brain). (**g**) Acute induction of *Rnf213* transcripts after intraperitoneal injections of IFNG and TNFA *in vivo*. (**a–g**) Data are shown as mean ± SD values from 3 or more independent assays and analyzed using Dunnett's test (**a**,**g**) Tukey's HSD test (**b**,**e**) and Student's t-test (**c**). $^{**}p < 0.01$, $^{***}p < 0.001$.

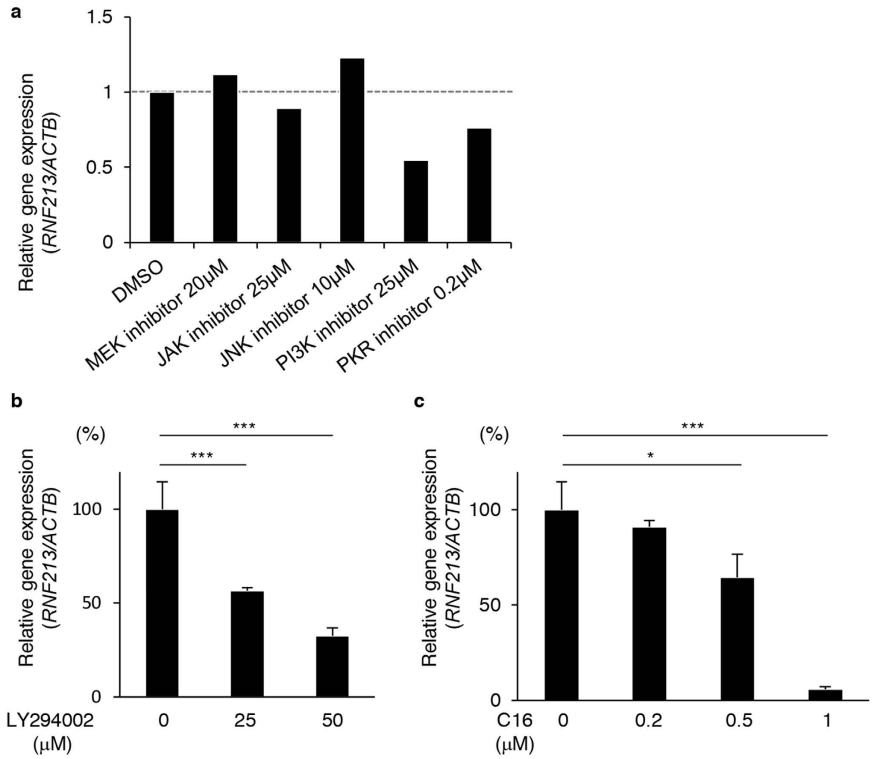

Figure 2. Phosphatidylinositol-4,5-bisphospate 3-kinase and double-stranded RNA-dependent protein kinase are the two upstream regulators of *RNF213* expression. (**a**) Plots show the relative expressions of *RNF213* mRNA in the presence or absence of protein kinase inhibitors for MEK (U0126, 20 μM), JAK (AG490, 25 μM), JNK (SP600125, 10 μM) and PI3K (LY294002, 25 μM) and PKR (C16, 0.2 μM). Mean values from two independent assays are shown. (**b**,**c**) Dose-dependent inhibition of *RNF213* induction by LY294002 (**b**) and C16 (**c**). Relative expressions of *RNF213* are plotted against various concentrations of PI3K and PKR inhibitors. Data are shown as values of mean ± SD from three independent assays and analyzed using Dunnett's test (**b**,**c**). *$p < 0.05$, ***$p < 0.001$.

upon IFNG treatment (Fig. 2a), and their inhibitory effects were dose-dependent (Fig. 2b,c). These data indicate that PI3K-AKT and PKR are two major upstream regulators of *RNF213* expression in endothelial cells, although it remains to be determined whether other unknown cascades might contribute to the transcriptional activation of *RNF213*.

RNF213 promotes endothelial cell proliferation. We next investigated the biological impacts of RNF213 depletion in endothelial cells. To identify downstream events, we tested whether siRNA-mediated knockdown of *RNF213* may lead to aberrant expressions of endogenously expressed genes in endothelial cells. Administration of siRNAs to *RNF213* (siRNF213#1 and #2) for 48 hr resulted in profound decrease in RNA (13–46%) and encoded protein (0%), indicating the efficient and rapid degradation of *RNF213* transcripts in the host cells within the time window (Supplementary Fig. S3). We next performed transcriptome analysis of HCAECs upon treatment with siRNF213#1 or with a control siRNA. Overall, a total of 217 genes were up-regulated (>2.0-fold change in expression), while 499 genes were down-regulated (<0.5-fold change in expression), in the siRNF213#1-treated cells when compared to the control (Supplementary Table S3 and Supplementary Table S4). The clustered gene matrix showed that differentially expressed genes between the test and control samples exhibited similar expression profiles within each group, indicating the high-confidence data of our transcriptome analysis (Fig. 3a).

To our surprise, a GO analysis highlighted the overrepresentation of cell cycle-associated genes among those aberrantly expressed in siRNA-treated HCAECs (Supplementary Table S3 and Supplementary Table S4). Specifically, "cell cycle process", "cell division", and "DNA replication" were listed among the top 5 GO categories (Supplementary Fig. S4). A KEGG pathway analysis also predicted that such gene expression changes might be linked to deregulation of cell cycle and its associated molecular pathways (Supplementary Fig. S5). Knowing that RNF213 might play an important role for cell-cycle progression in endothelial cells, we carried out the following three experiments to address this issue: First, quantitative (q) PCR assays successfully reproduced the microarray data. The expressions of *CCNA2*, *CCNB1* and *CCNE1* were decreased to 5.1% ($p = 0.0002$), 9.0% ($p = 0.0038$) and 28.1% ($p = 0.0006$) of control,

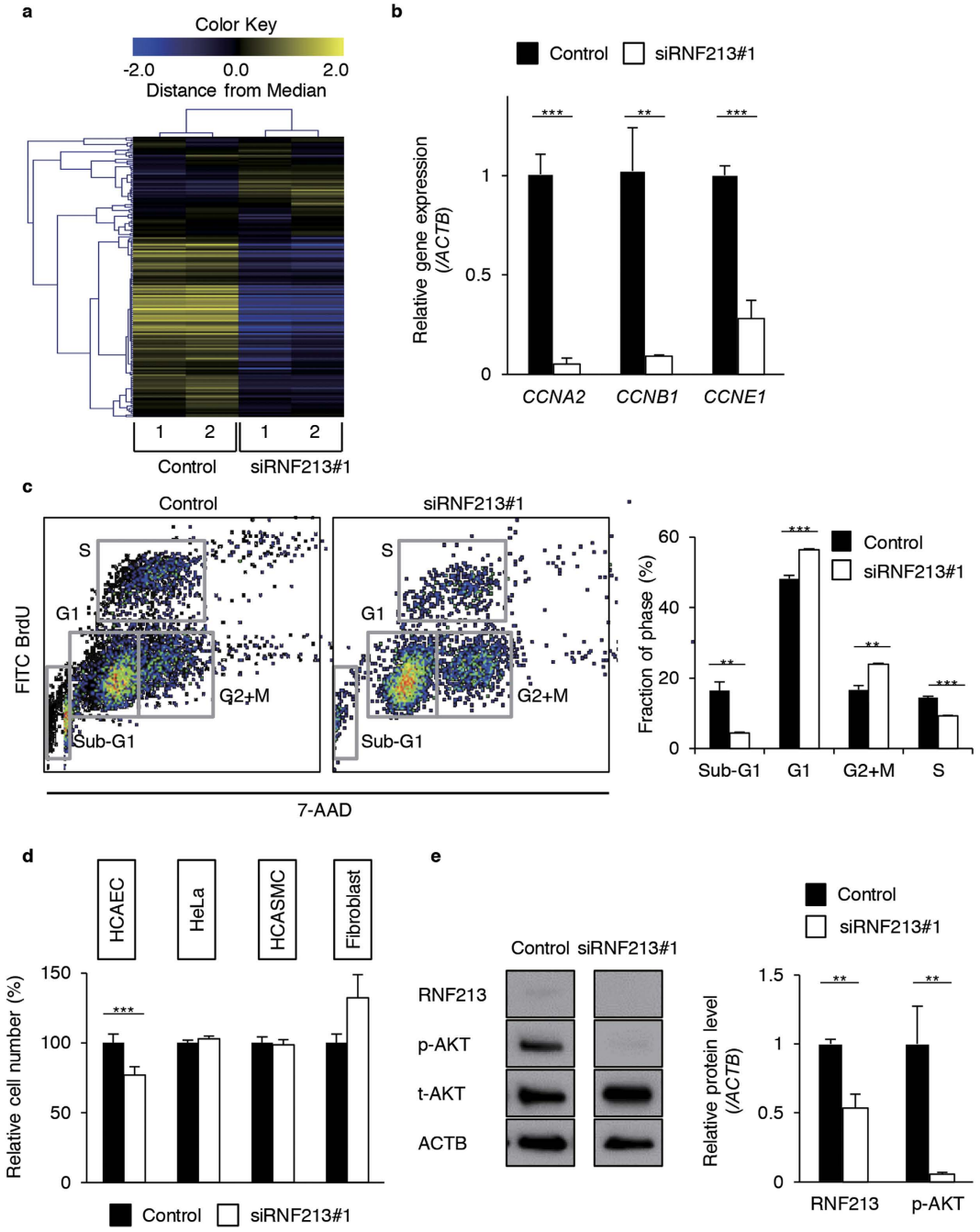

Figure 3. RNF213 up-regulates cell-cycle and proliferation of endothelial cells. (**a**) The heat map shows up (yellow) or down-regulated (blue) genes in siRNF213#1-treated or untreated HCAECs (n = 2 for each condition). Clustering of siRNA-treated cells and expression profiles for each experiment were conducted blindly. (**b**) Validating qPCR assays for *CCNA2*, *CCNB1* and *CCNE1* expressions in HUVECs with or without *RNF213* knockdown (mean ± SD, n = 3, using Student's t-test). $^{**}p < 0.01$, $^{***}p < 0.001$. (**c**) Flow-cytometry analysis for cell cycles of HUVECs. Used siRNAs (siRNF213#1 or control) are denoted at the top. The left two panels show 2D-plots for fluorescence intensity of FITC-labeled BrdU and that of 7-AAD. Fractions (%) of cells in G0/G1, S, G2+M and sub G0/G1-phases are indicated with squares. Bar plots on the right shows significant decrease in S-phase with siRNA-mediated knockdown of *RNF213* (n = 3, using Student's t-test, $^{***}p < 0.001$). (**d**) MTS assay for HCAECs, HeLa, HCASMCs and fibroblasts in the presence of *RNF213*-specific siRNA (siRNF213#1) or control siRNA (n = 3 in each group, using Student's t-test, $^{***}P < 0.001$). (**e**) Western blots for phosphorylated form of AKT (p-AKT), total AKT (t-AKT) and ACTB in HUVECs. Quantitative data from three independent Western blot analyses are shown as plots on the right (mean ± SD) and analyzed using Student's t-test. $^{**}p < 0.01$. Full length blots are presented in Supplementary Fig. S7.

respectively, when we knocked down *RNF213* in HUVECs (Fig. 3b). Second, flow cytometry analyses for BrdU- and 7-AAD-labeled cells revealed that knockdown of *RNF213* caused remarkable decline in the proportion of cells in S-phase (9.3 ± 0.2%), when compared to control cells (14.5 ± 0.4%, $p < 0.001$, Fig. 3c). In contrast, cells in static phases (G1 and G2+M) were significantly increased. The proportion of cells in Sub-G1 phase was decreased, indicating that apoptotic cells were not increased. Third, the MTS assays showed that *RNF213* knockdown led to a decrease in cell growth to 76.9 ± 5.9% of control in HCAECs ($p < 0.001$, Fig. 3d). In contrast, cell growths were not disturbed with siRNA treatments of non-endothelial cells, such as HeLa, HCASMCs or fibroblasts (Fig. 3d).

These data collectively provided evidence that RNF213 promotes cell proliferation through regulating its downstream pathways, and that endothelial cells are more susceptible to the functional loss of *RNF213* for cell growth than cells from other tissues. In agreement with these data, knockdown of *RNF213* was shown to decrease phosphorylated AKT (pAKT) in HUVECs and HCAECs, indicating lower activity of PI3K-AKT signal in endothelium. On the other hand, such difference was not observed in non-endothelial cells, HeLa, HCASMCs and fibroblasts (Fig. 3e, Supplementary Fig. S6 and Supplementary Fig. S7).

RNF213 is an upstream regulator of the matrix metalloproteinases. Cell growth-promoting signals, including the PI3K-AKT pathway, are reportedly associated with the angiogenic potential of endothelial cells[24]. This fact may support the cell-autonomous models of MMD, where functional deficits in endothelial RNF213 may lead to angiopathy as a consequence of persistently low PI3K-AKT activity. However, knowing that the endothelial AKT signals were not activated with the IFNG treatments (Supplementary Fig. S7), we hypothesized that RNF213 might mediate angiogenic responses of endothelial cells through PI3K-AKT-dependent and -independent mechanisms under inflammatory stresses. We therefore inspected minor changes in the microarray data searching for the genes that appeared to be independent of cell cycle and PI3K-AKT pathways.

We found, among aberrantly expressed genes and GO categories, that matrix metalloproteinase (MMP) genes were significantly up-regulated when *RNF213* was knocked down in endothelial cells (Supplementary Table S3). We therefore examined the expression changes of *MMPs* (*MMP1*, *2*, *3*, *8*, *10*, *11*, *14*, *15* and *17*) and of tissue inhibitors of metalloproteinases (*TIMP1* and *TIMP2*) upon knockdown of *RNF213* in HUVECs. A qPCR assays confirmed that all *MMPs* herein tested were elevated following *RNF213* silencing. We primarily focused on MMP1 because *MMP1* was the most prominently up-regulated gene among other *MMPs* with siRNA treatments to *RNF213* (Fig. 4a). This result was confirmed at the protein level when MMP1 protein level in the culture medium was measured by ELISA (Fig. 4b). Noticeably, such increase in *MMP1* expression was attenuated to 38.7% and 57.2% of control at the protein and RNA level, respectively, by pre-treatment with IFNG ($p < 0.001$, Fig. 4b,c). These results indicated that RNF213 controls the expressions of MMPs as an upstream regulator, and that RNF213 might play a potential role in angiogenesis through these effects on MMPs.

***RNF213* and *MMP1* expressions in fibroblasts from MMD patients.** To determine the relevance of above-described results to the pathogenic mechanisms of MMD, we asked whether the variant *RNF213* might have the properties of a hypomorphic allele. We used 4 fibroblasts from healthy volunteers and 2 from MMD patients. The 2 MMD fibroblast lines, but not the 4 controls, were heterozygous with the high-risk allele of *RNF213* (c.14756G>A) (Fig. 5a). In these lines, we confirmed that *RNF213* was similarly induced at mRNA level with IFNG treatments (Fig. 5b). The basal expression levels of *RNF213* as well as its response to the IFNG treatment did not differ between MMD and control groups (Fig. 5b).

We next compared the expressions of *MMP1* mRNA and protein in fibroblasts from MMD patients and healthy individuals. Surprisingly, one of fibroblasts from an MMD patient expressed higher amount of *MMP1* mRNA than controls ($p < 0.001$), while the other fibroblast did not show significant difference (Fig. 5c). Consequently, we obtained only a marginal difference in the *MMP1* expression between the MMD and control groups ($p = 0.052$, Fig. 5c). We observed the same trend for MMP1 protein (Supplementary Fig. S8). These data appeared to support that *MMP1* expression varies in individual fibroblasts regardless of the *RNF213* genotypes. Alternatively, however, it might be also possible that the variant *RNF213* allele could affect only minimally the gene expressions in fibroblasts and other non-endothelial cells. In fact, indispensable functions of RNF213 were observed only in endothelial cells (Fig. 4a,b).

We therefore suspected that *RNF213* might function as a dispensable molecule for regulating the *MMP1* expression in non-endothelial cells. To address this issue, we examined whether silencing of *RNF213* in fibroblasts might cause aberrant expressions of *MMP1*. As expected, *MMP1* mRNA expression was not altered with knockdown of *RNF213* in the fibroblasts from a healthy control (Fig. 5d). We further confirmed that IFNG treatment did not result in deregulation of *MMP1* expression in fibroblast in the presence of siRNA for *RNF213* (Fig. 5d). These results were substantially identical in independent assays using fibroblasts from other healthy controls and MMD patients (data not shown). Knockdown of *RNF213* did not alter the expressions of *MMP1* in HeLa or HCASMCs, either (Supplementary Fig. S9).

Endothelial RNF213 controls angiogenesis through regulating the expression of *MMP1*. Although *RNF213* have been shown to be essential for normal vascular development[12,25], it still remains unknown whether the angiogenic functions of RNF213 is associated with inflammatory signals.

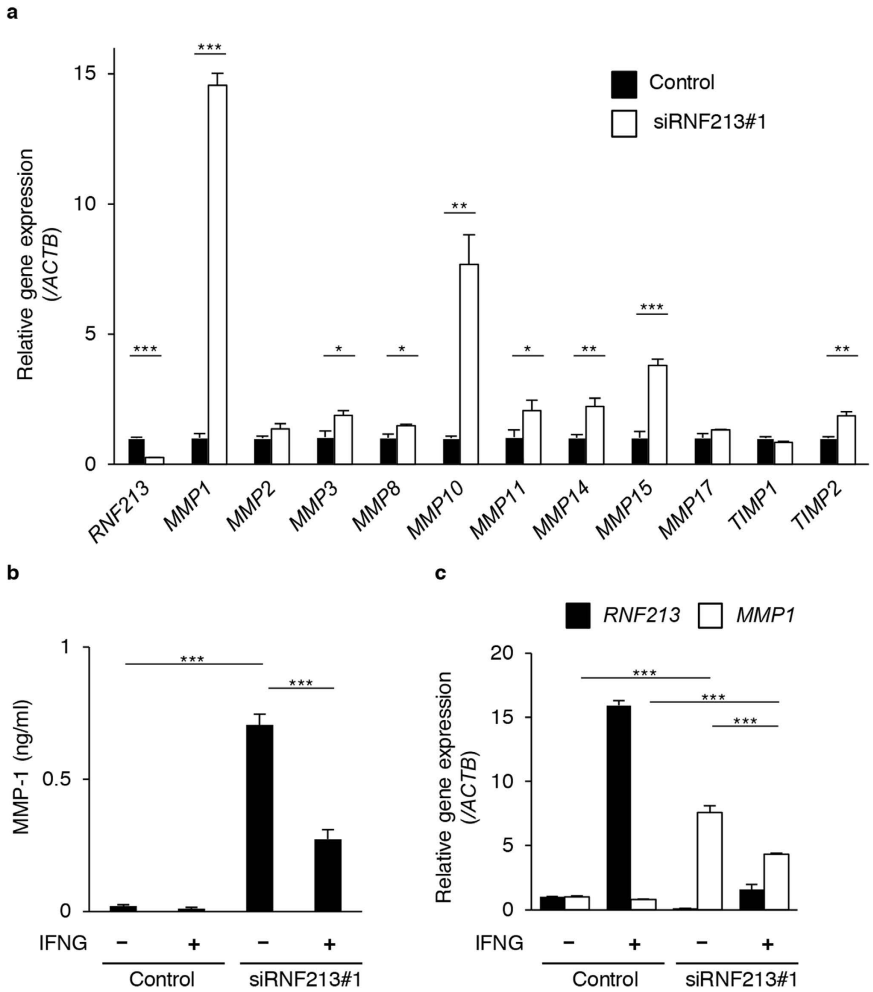

Figure 4. RNF213 controls the expression of MMPs in endothelial cells. (**a**) Relative expressions of *RNF213*, *MMPs*, *TIMP1* and *2* genes are plotted. Note the significant up-regulations of all but *MMP2*, *17*, *TIMP1* genes with knockdown of *RNF213* (white bars) compared to control experiments (black bars). Data are show as values of mean ± SD (n = 3) and analyzed using Student's t-test. *$p < 0.05$, **$p < 0.01$, ***$p < 0.001$. (**b**) Secreted MMP1 proteins in the culture medium. Data from three independent assays with ELISA are shown (mean ±SD). Note that MMP1 proteins are significantly elevated with knockdown of *RNF213* regardless of IFNG pretreatments. The elevation of MMP1 with *RNF213* knockdown are partly attenuated by IFNG pretreatments (IFNG+) compared to that in untreated cells (IFNG−), using Tukey's HSD test. ***$p < 0.001$. (**c**) Preventative effects of IFNG on aberrantly up-regulation of *MMP1* RNA due to *RNF213* knockdown. The data from three independent experiments followed by qPCR are shown and analyzed using Tukey's HSD test. ***$p < 0.001$.

As previously reported, the matrigel system showed rapid morphological changes of HUVECs and HCAECs into vascular structures within 8 hr after inoculation (Fig. 6a and Supplementary Fig. S10)[26]. Based on the previous data in this study, we predicted that functional loss of RNF213 or its upstream pathways might lead to deficits in such angiogenic responses. Indeed, we found that chemical inhibition of both PI3K-AKT and PKR pathways—the two upstream regulators of RNF213—efficiently disrupted angiogenesis (Supplementary Fig. S11 and Supplementary Fig. S12). Moreover, we found that angiogenic potentials of HUVECs and HCAECs were nearly completely ablated by the siRNA-mediated knockdown of *RNF213* both in presence and absence of IFNG pre-treatments (Fig. 6a and Supplementary Fig. S10).

Lastly, we determined if up-regulated MMPs might contribute to exaggerating the poor angiogenesis of HUVECs when *RNF213* was knocked down. To address this issue, we pretreated the cells for 48 hr with siRNA to knockdown the endogenous *RNF213*, and inoculated them onto the matrigels in the presence or absence of the MMP inhibitor, GM6001. We did find that the MMP inhibitor successfully restored the attenuated angiogenesis of HUVECs due to *RNF213* knockdown (0%) to 68.4% of control ($p = 0.02$, Fig. 6b,c). Furthermore, we confirmed that disrupted angiogenesis of HUVECs by PKR and PI3K inhibitors were nearly completely restored by GM6001 ($p < 0.001$, Fig. 6d,e). Therefore, RNF213 promoted angiogenesis of endothelial cells through both cell cycle-dependent and -independent

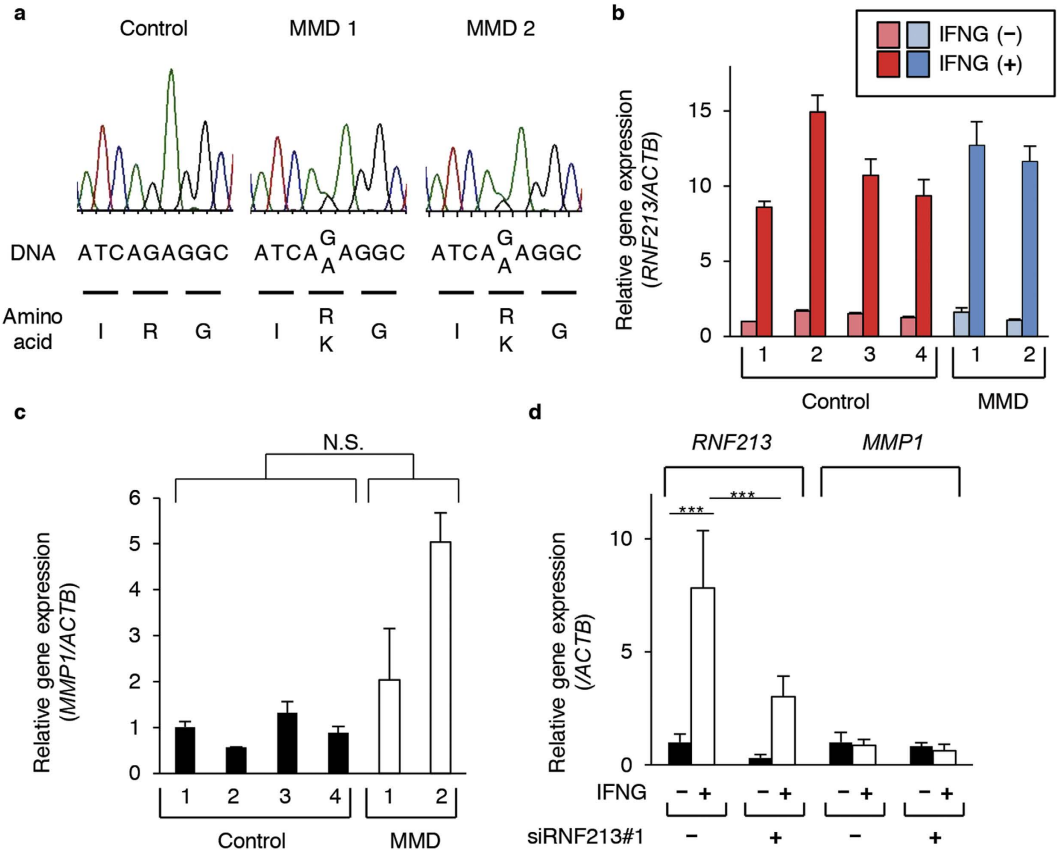

Figure 5. Comparative analysis of *MMP1* expressions in fibroblasts from healthy controls and MMD patients carrying the R4810K variant of *RNF213*. (**a**) Sanger sequences for the target region of *RNF213*. Note that healthy control (Normal) are have the wild-type allele, while two MMD patients (MMD1 and 2) carry a heterozygous c.14756G>A (R4810K) mutations. (**b**) Relative *RNF213* expressions and their responses to IFNG treatment in the fibroblasts from 4 healthy controls (Normal) and 2 MMD patients. Data are shown as mean ± SD values of qPCR assays in three independent assays. (**c**) Relative expressions of *MMP1* transcripts in fibroblasts from 4 individuals of healthy control and 2 MMD patients. Values are shown as mean ± SD (n = 3), and analyzed using Student's t-test. N.S., not significant. (**d**) Relative *RNF213* and *MMP1* expressions in control fibroblasts with or without treatment by IFNG and siRNF213#1 (mean ± SD, n = 3, using Tukey's HSD test, ***$p < 0.001$).

mechanisms. Among cell cycle-independent mechanisms, we identified MMP1 as one of the downstream effectors of RNF213 in endothelial cells for their angiogenic responses.

Taken together, we concluded that *RNF213* was inducible by cytokine-mediated signals in both endothelial and non-endothelial cells. By contrast, the key gene expression changes for angiogenic responses were specific to endothelial cells, but not common with non-endothelial cells.

Discussion

RNF213 has been recently identified as an MMD susceptibility gene, but the pathogenic mechanism and the functional implications of the variant allele encoding the R4810K-mutant protein remain unresolved[11,12]. In this study, we began by collating the expression profiles of *RNF213* from a massive set of transcriptomic data[16,27]. The unbiased, genome-wide approach successfully detected extremely high signals of co-expression profiles for *RNF213* in conjunction with other genes that were previously associated with inflammatory responses, pointing out *RNF213* as a candidate gene that plays a role in pathways such as "innate immune response (GO:0045087)", "positive regulation of I-kappaB kinase/NF-kappaB cascade (GO:0043123)" and "positive regulation of defense response to virus by host (GO:0002230)".

We thus explored to validate such bioinformatic predictions through biological experiments: First, we found that acute administrations of TNFA and co-stimulations with other pro-inflammatory cytokines dramatically induced transcription of *RNF213* both *in vivo* and *in vitro*. These data were particularly important in that RNF213 might potentially connect previously known environmental factors of MMD to cell-intrinsic models for the disease onset. Experiments with chemical inhibitors for both PKR and PI3K-AKT pathways efficiently blocked the transcriptional activation of *RNF213* after the cytokine treatment, indicating epistatic regulation of *RNF213* by these pathways. We therefore tested whether

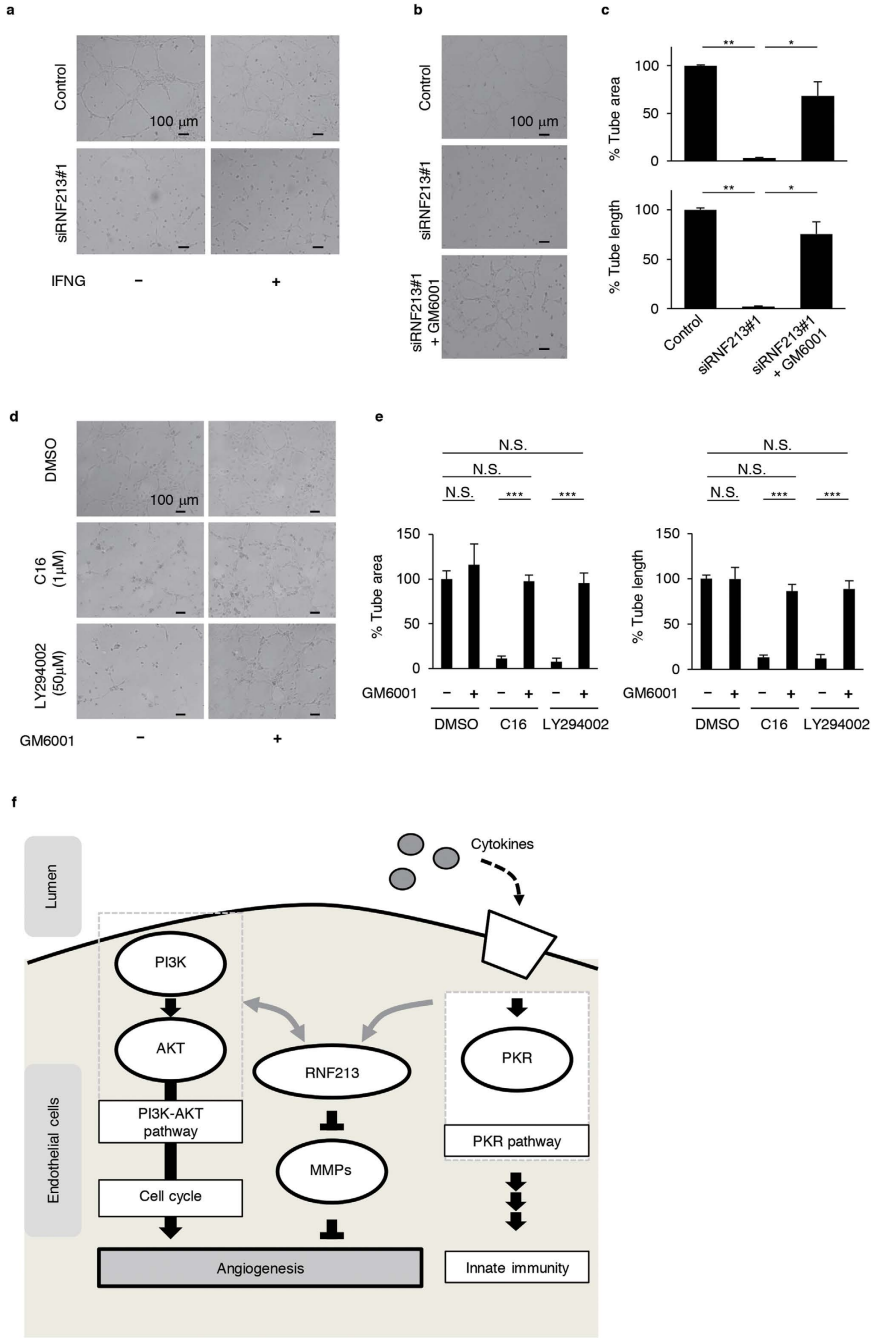

Figure 6. RNF213 links the external signals to angiogenesis through regulating *MMP1* expressions in endothelial cells. (**a**) The angiogenic responses of HUVECs on matrigels in different conditions. Representative images for tubular formation by trypsinized HUVECs in the absence (upper panels) or presence of siRNA for *RNF213* (lower). Effects of IFNG pretreatments (right) on angiogenic response of HUVECs are shown in comparison with those of untreated cells (left). Scale bar = 100 μm. (**b**) MMP is a key downstream molecule for deficits in angiogenic response of endothelial cells with depleted expression of *RNF213*. Upper, middle and lower panels show tubular formation of HUVECs on matrigel without siRNA treatment ("Control"), with siRNA-mediated knockdown of *RNF213* and with co-administration of GM6001, an MMP1 inhibitor, respectively. Scale bar = 100 μm. (**c**) The bar plots show quantitative results of % tube area (upper) and % tube length (lower) on matrigels using HUVECs (n = 3) for Fig. 6b. Tukey's HSD test. $^{*}p < 0.05$, $^{**}p < 0.01$. (**d**) Effects of PI3K and PKR inhibitors for tubular formations of HUVECs on the matrigel and its recovery by GM6001. Scale bar = 100 μm. (**e**) Bar plots presenting quantitative results of % tube area (left) and % tube length (right) on matrigels using HUVECs (n = 3) for Fig. 6d. Tukey's HSD test. $^{***}p < 0.001$. N.S., not significant. (**f**) A proposed model for the regulatory roles of RNF213, PI3K and PKR pathways in endothelial response to cytokines and in angiogenesis.

RNF213 and these molecular signals might interplay reciprocally in response to pro-inflammatory cytokines. SiRNA-mediated knockdown of *RNF213* in endothelial cells did not affect PKR or PI3K expression in response to TNFA and IFNG co-stimulations. On the other hand, *RNF213* knockdown led to remarkable decrease in phosphorylated AKT (pAKT) signals, as previously suggested[28]. These data clarified the following two points: 1) RNF213 is a downstream target, and not an upstream regulator, of cytokine-mediated PKR pathway; and 2) RNF213 and PI3K-AKT pathway reciprocally interact with or without cytokine stimulations.

Both PKR and PI3K-AKT pathways are major drivers of new protein synthesis, cell growth and autophagy[29,30]. Interestingly, endothelial autophagy is known to be essential for protecting endothelial cells from vascular insults and senescence[31]. In the present study, however, we were unable to obtain experimental data supporting the functional role of RNF213 in vascular autophagy (data not shown). Nonetheless, we anticipate that future experiments using *Rnf213*-knockout or its R4810K knock-in mice will provide robust evidence for these issues. The transcriptomic analysis on cultured endothelial cells in this study disclosed that siRNA-mediated knockdown of endogenous *RNF213* disturbed DNA synthesis and cell proliferation. These data supported an established concept that the cell-cycle progression of endothelial cells is correlated with their angiogenic properties[32]. Similarly, as the PI3K-AKT is a well-known pathway for cell growth, tumorigenesis and cancer-related angiogenesis[30], it is not surprising that the PI3K inhibitor LY294002 hampered the angiogenic phenotypes of endothelial cells in this study. Notably, we found that the PKR inhibitor also prevented *in vitro* angiogenesis. This finding recapitulated the modifying effects of PKR on angiogenesis through eIF2α phosphorylation[33]. We further found that the PKR inhibitor did not suppress the cell-cycle associated genes (data not shown). Together, it was suggested that RNF213 functions as a common downstream effector of PKR and PI3K-AKT pathways in endothelial angiogenesis through exerting its angiogenic effects through distinct molecular mechanisms in each pathway (Fig. 6f).

Based on an assumption that cell-cycle-independent mechanisms also contributed to the angiogenic defects as a consequence of RNF213 deficiency in endothelium, we closely inspected the minor findings in our microarray data. We found that several matrix metalloproteinase genes, including *MMP1*, *3*, *8*, *10*, *11*, *14*, *and 15*, were significantly increased in their expressions. Excessive MMPs are known to cause epithelial to mesenchymal transition, thereby leading to deleterious effects on endothelial cells in maintenance of vascular structures[34]. The MMP inhibitor, GM6001, restored abnormal phenotypes caused by siRNA-mediated *RNF213* silencing, indicating that the loss of *RNF213* was associated with active vascular remodeling through up-regulation of MMPs. These data indicated that RNF213 promoted angiogenesis through cell-cycle-dependent and independent mechanisms.

The knockdown experiments using fibroblasts did not recapitulate the data for over-expression of *MMP1* or downward regulation of PI3K-AKT that were observed for endothelial cells in this study. This discrepancy can be interpreted by hypothesizing that RNF213 promotes cell proliferation in endothelial cells, but not in other cells or tissues, through positive regulation of the PI3K-AKT pathway. From a more general perspective, these results may reflect differential roles of RNF213 in endothelial cells and other tissues including smooth muscle cells and fibroblasts. This perspective might be coherent with the fact that GO terms for co-expressed genes in the bioinformatic dataset did not necessarily overlap with those of our microarray data using endothelial cells.

In the present study, we also asked whether endothelial cell-autonomous models might fit better to the pathogenic processes of MMD than non-cell-autonomous models[35,36]. The elevated expressions of *MMP* mRNAs and proteins with reduced expression of *RNF213* in endothelial cells were likely to support the former, endothelial cell-autonomous model. We were unable to obtain direct evidence for higher expression of *MMP1* in vascular tissues from MMD patients. Alternative experiments applying combined methods of induced pluripotent stem cells with *in vitro* differentiation of endothelial cells will offer more clues for pathogenic responses of the cells from MMD patients to environmental signals. Considering previous studies that associated higher levels of plasma MMPs with increased risk of MMD[37,38] and increased vascular MMP-9 in mice lacking RNF213[39], we speculate that individuals with the R4810K mutation may have a tendency to produce higher amounts of MMPs from endothelial cells upon systemic inflammation.

A recent study identified *GUCY1A3*, which encodes the α1 subunit of soluble guanylate cyclase (sGC), the major receptor for nitric oxide (NO), as the gene mutated in a syndromic form of MMD[36]. This discovery implicated that alterations of NO-sGC pathway might lead to an abnormal vascular-remodeling process in sensitive vascular areas, such as internal carotid artery bifurcations. We surmised that this concept could be also valid with sporadic, non-syndromic forms of MMD. In line with this concept, it would be reasonable to test whether activated NO synthase under inflammatory stress may require RNF213 to down-regulate the production of MMPs.

One of remaining issues to discuss in this study was how the R4810K variant allele of *RNF213* could affect the biochemical function of RNF213—by a loss of function, gain-of function, or dominant mechanism? Since we were unable to observe differential MMP syntheses in fibroblasts from MMD patients when compared to those in healthy controls, we cannot safely conclude that the R4810K variant of RNF213 results in functional loss of the protein. Nonetheless, markedly elevated MMP production upon silencing of *RNF213* in endothelial cells led to deleterious effects on their angiogenic responses. In this

scenario, disease-susceptibility amino acid change (R4810K) is more likely linked to the functional deficiency of RNF213 than its gain of function.

Clinical implications of this study will be further strengthened by analyzing the functional roles of RNF213 in the context of vascular insults by virus and other pathogens. Knowing that the variant allele of *RNF213* appeared more frequently in individuals with syndromic forms of MMD than in the control group (our unpublished data), we assume that functional loss of RNF213 may contribute to the development of MMD even in the presence of other genetic causes or environmental risk factors, such as varicella zoster virus infection. Another aspect of clinical implications may include the potential therapeutic targets for MMD with MMP inhibitors. Also, given the active angiogenesis in malignant tissues and inhibitory effects of some MMPs on cancer proliferation, RNF213 could be considered as a target molecule for future cancer treatments[40].

In conclusion, our study provides new insight into the convergent functions of RNF213 among various genetic and environmental risk factors for the onset of MMD. We will use mouse models to further explore this issue and identify gene-environment interactions of the two main pathways related to RNF213 (PKR and PI3K-AKT) with vascular inflammation.

Methods

Bioinformatic search for co-expressed genes. Expression correlation analysis was performed as previously described[16,17]. Briefly, g:Profiler[41] retrieved a large amount of expression data for the most similarly co-expressed genes in a specified Gene Expression Omnibus (GEO, http://www.ncbi.nlm.nih.gov/geo/) dataset. Among them, expression data involving the four selected gene probes for *RNF213* (Affymetrix probes 225931, 230000, 232155 and 241347, Affymetrix, Santa Clara, CA, USA) was obtained from a total of 106 heterogeneous microarray experiments based on the human Affymetrix HG-U133 Plus 2.0 array. To associate highly correlated genes with specific categories of gene functions, Gene Ontology (GO) DAVID analysis (http://david.abcc.ncifcrf.gov/) were applied, and GO terms with more than a fold enrichment >2 and a P-value < 0.01 were retained (Supplementary Fig. S1 and Supplementary Table S1). Gene symbols and coordinates were used according to the UCSC genome browser hg19 (http://genome.ucsc.edu/). Protein domain information was obtained from Human Protein Reference Database (http://www.hprd.org/)[42].

Cell culture. Cells were purchased from ATCC (Manassas, VA, USA) and Coriell Institute (Camden, NJ, USA). Human coronary artery endothelial cells (HCAECs) were cultured in EGM-2MV (Lonza, Basel, Switzerland) containing 10% fetal calf serum (FCS)[43], and human umbilical vein endothelial cells (HUVECs) were cultured in EGM-2 (Lonza) containing 2% FCS[44]. Human coronary artery smooth muscle cells (HCASMCs) were cultured in SmGM-2 (Lonza) containing 5% FCS. HeLa cells and fibroblasts were cultured in Dulbecco's Minimal Essential Medium (Wako, Osaka, Japan) containing 10% FCS with 1% penicillin/streptomycin (Wako). HCAECs and HUVECs were assayed at passages 10 and 5, respectively. HCASMCs were assayed at passage 8. Fibroblasts were used at passage between 3 to 5. All cell cultures were maintained at 37 °C in normoxic environments with 5% CO_2 and 100% humidity.

Animal studies. Female C57 BL/6N mice at 4 weeks of ages were used for *in vivo* experiments. Briefly, 0.1 ml of PBS or 250 ng/body of TNFA (Sigma-Aldrich, Saint Louis, MO, USA) and 10 μg/body of IFNG (Sigma-Aldrich) were intraperitoneally injected. Animals were euthanized at 0, 6 and 24 hr after injection and RNA was immediately extracted from various tissues after sacrifice on deep anesthesia (RNeasy Micro Kit, Qiagen, Venlo, Netherlands). Total RNA was used for cDNA synthesis followed by quantitative PCR.

Quantitative real time PCR. Total RNA was extracted using RNeasy Micro Kit (Qiagen) and synthesized complementary DNA using High-Capacity RNA to cDNA Kit (Life Technologies, Carlsbad, CA, USA) according to the manufacturer's protocol. Quantitative real time PCR (qRT-PCR) was performed using Fast SYBR Green Master Mix and StepOnePlus (Life Technologies). Human *ACTB* or mouse *Actb* was used as internal control gene. The sequences of each gene specific primers were shown in Supplementary Table S2. The PCR conditions were 95 °C (20 seconds), 40 cycles of 95 °C (3 seconds), and 60 °C (30 seconds). Relative gene expression was calculated by ddCt method[43,45].

Western blotting. Cultured cells were lysed in Laemmli Sample Buffer (Biorad, Hercules, CA, USA). The total protein concentration in cell lysates was determined using Qubit 2.0 Fluorometer (Life Technologies). Equivalent protein amounts from each sample were separated by polyacrylamide gel electrophoresis using 4–15% Mini-PROTEAN TGX Gels (Biorad). Electrophoresed proteins were transfered to PVDF membranes (Trans-Blot Turbo Transfer Pack, Biorad). Blotted membranes were blocked with 5% milk and incubated at 4 °C for overnight with primary antibodies. Following antibodies were used: ACTB (1:10000; Abcam, Cambrige, United Kingdom), RNF213 (1:200; Sigma-Aldrich), AKT (1:1000; Cell Signaling Technology, Danvers, MA, USA), and phospho AKT (1:2000; Cell Signaling Technology). Light-chain specific anti-rabbit or mouse secondary antibodies conjugated to horseradish peroxidase (211-032-171 or 115-035-174, Jackson ImmunoResearch, West Grove, PA, USA) were used to detect

the specific protein signals. Chemiluminescence signals (ImmunoStar LD, Wako) were detected using FluorChem FC2 System (ProteinSimple, San Jose, CA, USA). ACTB was used as an internal control.

RNA interference. Transfection of small interfering RNA (siRNA) was conducted using Lipofectamine RNAiMAX (Life Technologies) according to the manufacturer's protocol. Commercially available siRNAs were used to knockdown human *RNF213*, which were herein designated as siRNF213#1 and #2 (Stealth RNAi #HSS126645 (sequences: 5′-UUUAACUGGCAUCUGUUUAAGGCCU-3′ and 5′-AGGCCUUAAACAGAUGCCAGUUAAA-3′) and #HSS184009 (sequences: 5′-UGAAGCAGCUGCCUCAACCCAUCUG-3′ and 5′-CAGAUGGGUUGAGGCAGCUGCUUCA-3′), respectively, Life Technologies). Stealth RNAi Negative Control Low GC Duplex (Life Technologies) was used for controls. To check knockdown of gene expression, qRT-PCR and western blotting were carried out as described above.

Microarray. Microarray-based transcriptome analyses for HCAECs were performed using Sure Print G3 Human GE microarray kit 8×60 k v2 (Agilent Technologies, Santa Clara, CA, USA), and the expression data were processed with GeneSpring GX software (Agilent Technologies) as previously described[43,45]. Bioinformatic analyses for clustering[46], GO and KEGG pathways (http://www.genome.jp/kegg/pathway.html) were conducted with standard protocols as described elsewhere[47–49]. Our transcriptome data have been deposited in NCBI Gene Expression Omnibus under accession code GSE62348.

Cell proliferation assay. The number of HUVECs was quantitatively analyzed on standard MTS assays using CellTiter 96 AQueous One Solution Cell Proliferation Assay (Promega, Madison, WI, USA). For S-phase specific labeling of growing cells, HUVECs were incubated in the presence of 10 μM BrdU for 2 hours. Cells were trypsinized and labeled with 7-Aminoactinomycin D, and then the proliferating cells in S phase were visualized with FITC BrdU Flow Kit (BD, Franklin Lakes, NJ, USA) using Epics XL (Beckman Coulter, Brea, CA, USA).

Angiogenic activity. Endothelial tube formation was assessed using Matrigel (BD) following to the manual. HUVECs or HCAECs were plated at 20,000 cells/well on matrigel-coated 24-well culture dishes. Cells were incubated for 4 hours at 37 °C and were allowed to form tube formations. For quantitation, tube area and length were calculated using Image J software (National Institutes of Health, Bethesda, MD, USA) as previously described[25].

ELISA and chemicals. Concentration of MMP-1 in the culture supernatant was measured with Quantikine ELISA (R&D Systems, Minneapolis, MN, USA) according to the manufacturer's protocol. Other chemicals were purchased from Sigma-Aldrich or Wako Pure Chemical Industries.

Statistical analysis. Results are shown as means ± standard deviation unless otherwise indicated. The statistical significance between groups was assessed by Student's t-test, Tukey's HSD test or Dunnett's test using JMP software (SAS Institute, Cary, NC, USA). The differences were considered significant when P values were less than 0.05.

Study approval. Ethical issues concerning this study were approved by the institutional review board at Kyushu University (#22-102). All subjects from MMD patients and healthy volunteers were provided with written forms of informed consent prior to this study. All procedures for animal experiments were approved by institutional review boards for animal care at Kyushu University (#A26-232-0). Experiments herein presented were all conducted in a stringent compliance to the institutional guideline.

References

1. Suzuki, J. & Takaku, A. Cerebrovascular "moyamoya" disease. Disease showing abnormal net-like vessels in base of brain. *Arch. Neurol.* **20,** 288–299 (1969).
2. Weinberg, D. G. *et al.* Moyamoya disease: a review of histopathology, biochemistry, and genetics. *Neurosurg. Focus* **30,** E20 (2011).
3. Ueno, M., Oka, A., Koeda, T., Okamoto, R. & Takeshita, K. Unilateral occlusion of the middle cerebral artery after varicella-zoster virus infection. *Brain Dev.* **24,** 106–108 (2002).
4. Tanigawara, T. *et al.* Studies on cytomegalovirus and Epstein-Barr virus infection in moyamoya disease. *Clin. Neurol. Neurosurg.* **99 Suppl 2,** S225–228 (1997).
5. Uchino, K., Johnston, S. C., Becker, K. J. & Tirschwell, D. L. Moyamoya disease in Washington State and California. *Neurology* **65,** 956–958 (2005).
6. Ikeda, H., Sasaki, T., Yoshimoto, T., Fukui, M. & Arinami, T. Mapping of a familial moyamoya disease gene to chromosome 3p24.2-p26. *Am. J. Hum. Genet.* **64,** 533–537 (1999).
7. Inoue, T. K., Ikezaki, K., Sasazuki, T., Matsushima, T. & Fukui, M. Linkage analysis of moyamoya disease on chromosome 6. *J. Child Neurol.* **15,** 179–182 (2000).
8. Sakurai, K. *et al.* A novel susceptibility locus for moyamoya disease on chromosome 8q23. *J. Hum. Genet.* **49,** 278–281 (2004).
9. Yamauchi, T. *et al.* Linkage of Familial Moyamoya Disease (Spontaneous Occlusion of the Circle of Willis) to Chromosome 17q25. *Stroke* **31,** 930–935 (2000).
10. Liu, W. *et al.* A rare Asian founder polymorphism of Raptor may explain the high prevalence of Moyamoya disease among East Asians and its low prevalence among Caucasians. *Environ. Health Prev. Med.* **15,** 94–104 (2010).

11. Kamada, F. *et al.* A genome-wide association study identifies RNF213 as the first Moyamoya disease gene. *J. Hum. Genet.* **56,** 34–40 (2011).
12. Liu, W. *et al.* Identification of RNF213 as a susceptibility gene for moyamoya disease and its possible role in vascular development. *PloS ONE* **6,** e22542 (2011).
13. Morito, D. *et al.* Moyamoya disease-associated protein mysterin/RNF213 is a novel AAA+ ATPase, which dynamically changes its oligomeric state. *Sci. Rep.* **4,** 4442 (2014).
14. Ito, A. *et al.* Enhanced post-ischemic angiogenesis in mice lacking RNF213; a susceptibility gene for moyamoya disease. *Brain Res.* **1594,** 310–320 (2015).
15. Hitomi, T. *et al.* The moyamoya disease susceptibility variant RNF213 R4810K (rs112735431) induces genomic instability by mitotic abnormality. *Biochem. Biophys. Res. Commun.* **439,** 419–426 (2013).
16. Sardiello, M. *et al.* A gene network regulating lysosomal biogenesis and function. *Science* **325,** 473–477 (2009).
17. Gennarino, V. A. *et al.* MicroRNA target prediction by expression analysis of host genes. *Genome Res.* **19,** 481–490 (2009).
18. Tanaka, Y. *et al.* Anti-viral protein APOBEC3G is induced by interferon-α stimulation in human hepatocytes. *Biochem. Biophys. Res. Commun.* **341,** 314–319 (2006).
19. Leibovich, S. J. *et al.* Macrophage-induced angiogenesis is mediated by tumor necrosis factor-α. *Nature* **329,** 630–632 (1987).
20. Numasaki, M., Lotze, M. T. & Sasaki, H. Interleukin-17 augments tumor necrosis factor-α-induced elaboration of proangiogenic factors from fibroblasts. *Immunol* Lett. **93,** 39–43 (2004).
21. Faggioli, L. *et al.* Molecular mechanisms regulating induction of interleukin-6 gene transcription by interferon-γ. *Eur J Immunol.* **27,** 3022–3030 (1997).
22. Lee, C. M. *et al.* Phosphatidylinositol 3-kinase inhibition by LY294002 radiosensitizes human cervical cancer cell lines. *Clin. Cancer Res.* **12,** 250–256 (2006).
23. Shimazawa, M. & Hara, H. Inhibitor of double stranded RNA-dependent protein kinase protects against cell damage induced by ER stress. *Neurosci. Lett.* **409,** 192–195 (2006).
24. Karar, J. & Maity, A. PI3K/AKT/mTOR Pathway in Angiogenesis. *Front. Mol. Neurosci.* **4,** 51 (2011).
25. Hitomi, T. *et al.* Downregulation of Securin by the variant RNF213 R4810K (rs112735431, G>A) reduces angiogenic activity of induced pluripotent stem cell-derived vascular endothelial cells from moyamoya patients. B*iochem. Biophys. Res. Commun.* **438,** 13–19 (2013).
26. Shi, F. *et al.* Effects of simulated microgravity on human umbilical vein endothelial cell angiogenesis and role of the PI3K-Akt-eNOS signal pathway. *PloS ONE* **7,** e40365 (2012).
27. Gennarino, V. A. *et al.* Identification of microRNA-regulated gene networks by expression analysis of target genes. *Genome Res.* **22,** 1163–1172 (2012).
28. Dai, D. *et al.* Serum miRNA Signature in Moyamoya Disease. *PloS ONE* **9,** e102382 (2014).
29. Nakamura, H. *et al.* Regulation of herpes simplex virus gamma(1)34.5 expression and oncolysis of diffuse liver metastases by Myb34.5. *J. Clin. Invest.* **109,** 871–882 (2002).
30. Kondo, Y., Kanzawa, T., Sawaya, R. & Kondo, S. The role of autophagy in cancer development and response to therapy. *Nat. Rev. Cancer* **5,** 726–734 (2005).
31. Peng, N. *et al.* An activator of mTOR inhibits oxLDL-induced autophagy and apoptosis in vascular endothelial cells and restricts atherosclerosis in apolipoprotein E(−)/(−) mice. *Sci. Rep.* **4,** 5519 (2014).
32. Zhang, Y., Griffith, E. C., Sage, J., Jacks, T. & Liu, J. O. Cell cycle inhibition by the anti-angiogenic agent TNP-470 is mediated by p53 and p21WAF1/CIP1. *Proc. Nat. Acad. Sci. USA* **97,** 6427–6432 (2000).
33. Papadakis, A. I. *et al.* eIF2α Kinase PKR modulates the hypoxic response by Stat3-dependent transcriptional suppression of HIF-1α. *Cancer Res.* **70,** 7820–7829 (2010).
34. Kovacic, J. C., Mercader, N., Torres, M., Boehm, M. & Fuster, V. Epithelial-to-mesenchymal and endothelial-to-mesenchymal transition: from cardiovascular development to disease. *Circulation* **125,** 1795–1808 (2012).
35. Sonobe, S. *et al.* Temporal profile of the vascular anatomy evaluated by 9.4-T magnetic resonance angiography and histopathological analysis in mice lacking RNF213: a susceptibility gene for moyamoya disease. *Brain Res.* **1552,** 64–71 (2014).
36. Herve, D. *et al.* Loss of α1β1 soluble guanylate cyclase, the major nitric oxide receptor, leads to moyamoya and achalasia. *Am. J. Hum. Genet.* **94,** 385–394 (2014).
37. Kang, H. S. *et al.* Plasma matrix metalloproteinases, cytokines and angiogenic factors in moyamoya disease. *J. Neurol. Neurosurg. Psychiatry* **81,** 673–678 (2010).
38. Fujimura, M., Watanabe, M., Narisawa, A., Shimizu, H. & Tominaga, T. Increased expression of serum Matrix Metalloproteinase-9 in patients with moyamoya disease. *Surg. Neurol.* **72,** 476–480; discussion 480 (2009).
39. Sonobe, S. *et al.* Increased vascular MMP-9 in mice lacking RNF213: moyamoya disease susceptibility gene. *Neuroreport* **25,** 1442–1446 (2014).
40. Kessenbrock, K., Plaks, V. & Werb, Z. Matrix metalloproteinases: regulators of the tumor microenvironment. *Cell* **141,** 52–67 (2010).
41. Reimand, J., Kull, M., Peterson, H., Hansen, J. & Vilo, J. g:Profiler—a web-based toolset for functional profiling of gene lists from large-scale experiments. *Nucleic Acids Res.* **35,** W193–200 (2007).
42. Keshava Prasad, T. S. *et al.* Human Protein Reference Database—2009 update. *Nucleic Acids Res.* **37,** D767–772 (2009).
43. Nishio, H. *et al.* Nod1 ligands induce site-specific vascular inflammation. *Arterioscler. Thromb. Vasc. Biol.* **31,** 1093–1099 (2011).
44. Bala, K., Ambwani, K. & Gohil, N. K. Effect of different mitogens and serum concentration on HUVEC morphology and characteristics: implication on use of higher passage cells. *Tissue Cell* **43,** 216–222 (2011).
45. Ikeda, K. *et al.* Unique activation status of peripheral blood mononuclear cells at acute phase of Kawasaki disease. *Clin. Exp. Immunol.* **160,** 246–255 (2010).
46. Eisen, M. B., Spellman, P. T., Brown, P. O. & Botstein, D. Cluster analysis and display of genome-wide expression patterns. *Proc. Nat. Acad. Sci. USA* **95,** 14863–14868 (1998).
47. Ashburner, M. *et al.* Gene ontology: tool for the unification of biology. The Gene Ontology Consortium. *Nat. Genet.* **25,** 25–29 (2000).
48. Kanehisa, M. *et al.* Data, information, knowledge and principle: back to metabolism in KEGG. *Nucleic Acids Res.* **42,** D199–205 (2014).
49. Kanehisa, M. & Goto, S. KEGG: Kyoto Encyclopedia of Genes and Genomes. *Nucleic Acids Res.* **28,** 27–30 (2000).

Acknowledgments

We thank Tamami Tanaka, Ayumi Tahara and Kaori Yasuda (cell innovator) for technical supports. This study was supported in part by KAKEN # 24650199 and 15K09624 (awarded to Y.S.), Japan Life Science Foundation (Y.S.), Takeda Science Foundation (Y.S.), The Japan Epilepsy Research Foundation (Y.S.), and The Mother and Child Health Foundation (Y.S.).

Author Contributions

K.O., Y.S., M. Sardiello, T.H. wrote the paper. K.O. carried out most parts of experiments and M. Sardiello performed the bioinformatics analyses. Y.S. directed the experiments and supervised the manuscript preparation. H.I., S.A., Y.I., Y.M., M. Sanefuji, H.T. technically assisted the experimental works. K.I. and T.H. contributed to the grand design of this study. All authors reviewed the manuscript.

Additional Information

Accession codes: Our transcriptome data have been deposited in NCBI Gene Expression Omnibus under accession code GSE62348.

Supplementary information accompanies this paper at http://www.nature.com/srep

Competing financial interests: The authors declare no competing financial interests.

How to cite this article: Ohkubo, K. *et al.* Moyamoya disease susceptibility gene *RNF213* links inflammatory and angiogenic signals in endothelial cells. *Sci. Rep.* **5**, 13191; doi: 10.1038/srep13191 (2015).

Supplementary Information for

Moyamoya disease susceptibility gene *RNF213* links inflammatory and angiogenic signals in endothelial cells

Kazuhiro Ohkubo[1,†], Yasunari Sakai[1,*,†], Hirosuke Inoue[1], Satoshi Akamine[1], Yoshito Ishizaki[1], Yuki Matsushita[1], Masafumi Sanefuji[1], Hiroyuki Torisu[1,3], Kenji Ihara[1,2], Marco Sardiello[4] & Toshiro Hara[1]

1. Department of Pediatrics, Graduate School of Medical Sciences, Kyushu University, Fukuoka 812-8582, Japan
2. Department of Pediatrics, Faculty of Medicine, Oita University, Yufu 879-5593, Japan
3. Section of Pediatrics, Department of Medicine, Fukuoka Dental College, Fukuoka 814-0193, Japan
4. Department of Molecular and Human Genetics, Baylor College of Medicine, Jan and Dan Duncan Neurological Research Institute, Texas Children's Hospital, Houston 77030, USA

*Correspondence to: Yasunari Sakai, M.D., Ph.D.

Department of Pediatrics, Graduate School of Medical Sciences,
Kyushu University
3-1-1 Maidashi, Higashi-ku, Fukuoka 812-8582, Japan.
Phone + 81-92-642-5421

Fax +81-92-642-5435

E-mail: ysakai22q13@gmail.com

†These authors contributed equally to this work

This material contains the following items:

- Supplementary Tables S1-4
- Supplementary Figures S1-12 with legends

Supplementary Table S1 | Gene ontology analysis for the genes co-expressed with *RNF213 in silico.*

GO Accession	GO Term	P-Value	Fold Enrichment	Related Genes
GO:0006955	immune response	2.19E-21	7.04	PSMB10, IFIH1, IFITM3, CCR1, OAS3, RSAD2, OAS1, APOBEC3G, IFI44L, OAS2, CXCL11, IFI35, CXCL10, CD97, TAP2, TAP1, DHX58, FYB, GBP5, SP100, BST2, LYN, CFB, SERPING1, SLAMF7, HLA-E, TRIM22, HLA-F, PSMB9, DDX58, OASL, TNFSF10, APOL1, TNFSF13B, GBP4, GBP2, GBP1
GO:0009615	response to virus	1.20E-19	22.89	IFIH1, BST2, RSAD2, APOBEC3G, IFI44, IFI16, STAT1, TRIM22, IFI35, ISG20, STAT2, DDX58, IRF9, PLSCR1, ISG15, IRF7, MX1, EIF2AK2, MX2
GO:0006952	defense response	2.70E-12	5.55	IFIH1, NMI, CCR1, RSAD2, APOBEC3G, CXCL11, CXCL10, CD97, LGALS3BP, TAP2, TAP1, MX1, MX2, DHX58, SP100, LYN, CFB, SERPING1, SLAMF7, IDO1, APOL2, DDX58, APOL3, SIGLEC1, APOL1, IRF7
GO:0006954	inflammatory response	5.88E-06	5.25	NMI, LYN, CFB, CCR1, SERPING1, IDO1, CXCL11, CXCL10, CD97, APOL2, SIGLEC1, APOL3, IRF7
GO:0045087	innate immune response	9.37E-06	8.57	DDX58, IFIH1, APOL1, SP100, CFB, APOBEC3G, SERPING1, SLAMF7, DHX58
GO:0009611	response to wounding	1.70E-04	3.47	NMI, LYN, CFB, CCR1, SERPING1, IDO1, CXCL11, CXCL10, CD97, APOL2, APOL3, PLSCR1, SIGLEC1, IRF7
GO:0002230	positive regulation of defense response to virus by host	5.55E-04	78.80	DDX58, PML, APOBEC3G
GO:0043123	positive regulation of I-kappaB kinase/NF-kappaB cascade	8.22E-04	8.12	TRIM38, APOL3, CFLAR, TNFSF10, BST2, CASP1

Supplementary Table S2 | Oligonucleotide primers for qPCR assays.

Gene	Forward Primer	Reverse Primer
ACTB	5’-CACCCTGAAGTACCCCATCG-3’	5’-TGCCAGATTTTCTCCATGTCG-3’
RNF213	5’-AACAGCTATTCCGTGGATGC-3’	5’-CCAGAGTGGGTATTCCCTTG-3’
LGALS3BP	5’-CATGAGTGTGGATGCTGAGT-3’	5’-CAGCTTGTGGAAGCACTTG-3’
PSMB9	5’-AGAAGTCCACACCGGGACCAC-3’	5’-TGTCAAACACTCGGTTCACCA-3’
TAP1	5’-TGGTCTGTTGACTCCCTTACAC-3’	5’-AAATACCTGTGGCTCTTGTCC-3’
APOBEC3G	5’-CCGAGGACCCGAAGGTTAC-3’	5’-TCCAACAGTGCTGAAATTCG-3’
IFIH	5’-ATGGAAAAAAAAGCTGCAAAAGA-3’	5’-GTACTTCCTCAAATGTTCTGCACAA-3’
BST2	5’-TTCTCAGTCGCTCCACCT-3’	5’-CACCTGCAACCACACTGT-3’
STAT1	5’-AACGGAGGCGAACCTGACTTCCA-3’	5’-GGCCTGGAGTAATACTTTCCAA-3’
CFB	5’-TGGAAAACCTGGAAGATGTTT-3’	5’-GGTTGCTTGTGGTAATCGGT-3’
TAP2	5’-TACAACACCCGCCATCAG-3’	5’-AGGTCTCTCCGCCAATACAG-3’
ISG15	5’-GGACAAATGCGACGAACCTCT-3’	5’-GGCCTGGAGTAATACTTTCCAA-3’
MX2	5’-CAGCCACCACCAGGAAACA-3’	5’-TTCTGCTCGTACTGGCTGTACAG-3’
TRIM22	5’-GGTTGAGGGGATCGTCAGTA-3’	5’-TTGGAAACAGATTTTGGCTTC-3’
DDX58	5’-GACTGGACGTGGCAAAACAA-3’	5’-TTGAATGCATCCAATATACACTTCTG-3’
IFIT1	5’-GCCATTTTCTTTGCTTCCCCTA-3’	5’-TGCCCTTTTGTAGCCTCCTTG-3’
IRF7	5’-CAGCGTCGGTGGCTACAA-3’	5’-CGCAGCGGAAGTTGGTTTT-3’
IL6	5’-CCACACAGACAGCCACTCAC-3’	5’-AGGTTGTTTTCTGCCAGTGC-3’

Supplementary Table S2 | Oligonucleotide primers for qPCR assays. (continued)

Gene	Forward Primer	Reverse Primer
CCNA2	5’-TCCAAGAGGACCAGGAGAATATCA-3’	5’-TCCTCATGGTAGTCTGGTACTTCA-3’
CCNB1	5’-GAAGATCAACATGGCAGGCG-3’	5’-GCATTTTGGCCTGCAGTTGT-3’
CCNE1	5’-TTCTTGAGCAACACCCTCTTCTGCAGCC -3’	5’-TCGCCATATACCGGTCAAAGAAATCTTGTGCC -3’
MMP1	5’-ATGCTGAAACCCTGAAGGTG-3’	5’-GAGCATCCCCTCCAATACCT-3’
MMP2	5’-GGCCCTGTCACTCCTGAGAT-3’	5’-GGCATCCAGGTTATCGGGGA-3
MMP3	5’-GTCTCTTTCACTCAGCCAAC-3’	5’-ATCAGGATTTCTCCCCTCAG-3’
MMP8	5’-TGATGAAAAAGCCTCGCTG-3’	5’-TGTTGATATCTGCCTCTCCC-3’
MMP10	5’-CATTCCTTGTGCTGTTGTGTC-3’	5’-TGTCTAGCTTCCCTGTCACC-3’
MMP11	5’-AGACACCAATGAGATTGCAC-3’	5’-GCACCTTGGAAGAACCAAATG-3’
MMP14	5’-CGCTACGCCATCCAGGGTCTCAAA -3’	5’-CGGTCATCATCGGGCAGCACAAAA-3’
MMP15	5’-ACAACTATCCCATGCCCATC-3’	5’-ACCTGTCCTCTTGGAAGAAG-3’
MMP17	5’-TCCAGATCGACTTCTCCAAG-3’	5’-CCACATGGCTTAACCCAATG-3’
TIMP1	5’-GGGCTTCACCAAGACCTA-3’	5’-GAAGAAAGATGGGAGTGGG-3’
TIMP2	5’-CCAAAGCGGTCAGTGAGA-3’	5’-TGGTGCCCGTTGATGTTC-3’
mouse Actb	5’-GGCTGTATTCCCCTCCATCG-3’	5’-CCAGTTGGTAACAATGCCATGT-3’
mouse Rnf213	5’-TAAGGATGTCCGCTCCTGGTT-3’	5’-TTGATGGCAGTATACTTGGCA-3’

Supplementary Table S3 | Up-regulated genes with siRNA-mediated knockdown of *RNF213* in HCAECs (top100).

Order of Gene	GeneSymbol	RefSeq Accession	Z score	Order of Gene	GeneSymbol	RefSeq Accession	Z score
1	UBD	NM_006398	6.45	51	TP53I3	NM_004881	3.17
2	SELE	NM_000450	5.83	52	SULF2	NM_018837	3.17
3	HMOX1	NM_002133	5.66	53	BTG2	NM_006763	3.14
4	LCN15	NM_203347	5.64	54	TP53I3	NM_004881	3.13
5	GALNT7	NM_017423	4.98	55	ZNF219	NM_016423	3.12
6	MRC1	NM_002438	4.98	56	RASSF2	NM_014737	3.12
7	IL4I1	NM_172374	4.96	57	SLC6A16	NM_014037	3.11
8	TRAF1	NM_005658	4.92	58	TMEM132A	NM_017870	3.11
9	MT1F	NM_005949	4.90	59	MMP1	NM_002421	3.08
10	ADAM9	NM_003816	4.74	60	CDO1	NM_001801	3.06
11	KALRN	NM_003947	4.61	61	FAM104A	NM_032837	3.01
12	BIRC3	NM_001165	4.47	62	NRP1	NM_003873	3.01
13	IL8	NM_000584	4.32	63	PRCP	NM_199418	3.01
14	KITLG	NM_000899	4.24	64	FBLL1	NR_024356	3.00
15	VWF	NM_000552	4.05	65	CLDN5	NM_001130861	2.99
16	ZMAT3	NM_022470	4.00	66	CH25H	NM_003956	2.98
17	PLA2G4C	NM_003706	3.95	67	NID1	NM_002508	2.96
18	PSG8	NM_001130167	3.94	68	SNN	NM_003498	2.95
19	LDHB	NM_002300	3.93	69	IL32	NM_001012633	2.89
20	LTB	NM_002341	3.90	70	HIST1H4K	NM_003541	2.87
21	FAS	NM_000043	3.83	71	NEURL3	NR_026875	2.86
22	TSPAN11	NM_001080509	3.76	72	RNF13	NM_007282	2.83
23	VWCE	NM_152718	3.76	73	COL1A2	NM_000089	2.83
24	NUAK2	NM_030952	3.74	74	SLC40A1	NM_014585	2.83
25	SLC7A7	NM_001126106	3.71	75	TMEM217	NM_001162900	2.83
26	CLNS1A	NM_001293	3.71	76	CTSK	NM_000396	2.82
27	ARL6IP1	NM_015161	3.69	77	ICAM1	NM_000201	2.82
28	CXorf36	NM_024689	3.66	78	RAG1	NM_000448	2.81
29	FAS	NM_000043	3.65	79	LRRC8B	NM_015350	2.81
30	MT1M	NM_176870	3.64	80	ID2	NM_002166	2.81
31	FAS	NM_000043	3.57	81	USP46	NM_022832	2.79
32	CEACAM1	NM_001712	3.54	82	CLN8	NM_018941	2.79
33	MMP10	NM_002425	3.51	83	GPIHBP1	NM_178172	2.76
34	PSG2	NM_031246	3.51	84	KLHDC9	NM_001007255	2.74
35	FAM49B	NM_016623	3.50	85	NUPR1	NM_001042483	2.74
36	NID2	NM_007361	3.48	86	SEMA6C	NM_001178061	2.74
37	CSF2	NM_000758	3.43	87	LOC282997	NR_026932	2.71
38	SLC2A3	NM_006931	3.43	88	ID2	NM_002166	2.71
39	PLTP	NM_006227	3.43	89	GPR116	NM_001098518	2.69
40	MT1E	NM_175617	3.42	90	C9orf80	NM_021218	2.69
41	MAP2	NM_002374	3.41	91	LRRC8B	NM_015350	2.69
42	ICK	NM_016513	3.38	92	RPL22	NM_000983	2.67
43	C6orf192	NM_052831	3.37	93	ATL1	NM_181598	2.67
44	PSG8	NM_182707	3.33	94	ACP5	NM_001611	2.63
45	CCL2	NM_002982	3.27	95	C20orf108	NM_080821	2.61
46	IL32	NM_001012631	3.26	96	RAB8B	NM_016530	2.60
47	LDHB	NM_001174097	3.25	97	GPR116	NM_001098518	2.53
48	C7orf41	NM_152793	3.21	98	SIRPB2	NM_001122962	2.52
49	GPR116	NM_001098518	3.20	99	RELB	NM_006509	2.48
50	FZD4	NM_012193	3.19	100	GDF15	NM_004864	2.40

MMPs were highlighted in red.

Supplementary Table S4 | Down-regulated genes with siRNA-mediated knockdown of *RNF213* in HCAECs (top100).

Order of Gene	GeneSymbol	RefSeq Accession	Z score	Order of Gene	GeneSymbol	RefSeq Accession	Z score
1	E2F2	NM_004091	-5.96	51	CDCA8	NM_018101	-4.49
2	FAM167A	NM_053279	-5.80	52	CDC20	NM_001255	-4.49
3	CENPA	NM_001809	-5.80	53	PLK1	NM_005030	-4.48
4	ITGB4	NM_000213	-5.77	54	NUF2	NM_145697	-4.48
5	MKI67	NM_002417	-5.49	55	ANLN	NM_018685	-4.47
6	TOP2A	NM_001067	-5.44	56	CCNA2	NM_001237	-4.47
7	MKI67	NM_002417	-5.38	57	CDKN3	NM_005192	-4.46
8	RPL22L1	NM_001099645	-5.38	58	CDCA5	NM_080668	-4.45
9	KIFC1	NM_002263	-5.37	59	TROAP	NM_005480	-4.43
10	UBE2C	NM_181803	-5.36	60	DIAPH3	NM_030932	-4.42
11	KIF20A	NM_005733	-5.34	61	KIF23	NM_138555	-4.40
12	RRM2	NM_001034	-5.29	62	MKI67	NM_002417	-4.40
13	PRC1	NM_003981	-5.24	63	FAM64A	NM_001195228	-4.39
14	MSMP	NM_001044264	-5.17	64	ASF1B	NM_018154	-4.38
15	H2AFV	NM_012412	-5.17	65	MND1	NM_032117	-4.38
16	RAD54L	NM_003579	-5.11	66	EGR1	NM_001964	-4.38
17	KIF15	NM_020242	-5.08	67	SGOL1	NM_001012409	-4.36
18	NTSR1	NM_002531	-4.99	68	BUB1B	NM_001211	-4.35
19	ASPM	NM_018136	-4.96	69	CDCA7L	NM_018719	-4.32
20	CDC25C	NM_001790	-4.96	70	TGM2	NM_198951	-4.32
21	CENPM	NM_024053	-4.92	71	PTTG1	NM_004219	-4.31
22	KIF2C	NM_006845	-4.90	72	CDKN3	NM_005192	-4.29
23	XRCC6	NM_001469	-4.89	73	CCNB1	NM_031966	-4.29
24	ASPM	NM_018136	-4.87	74	CDK1	NM_001786	-4.29
25	SPC25	NM_020675	-4.81	75	DKK2	NM_014421	-4.24
26	IQGAP3	NM_178229	-4.80	76	SKA1	NM_001039535	-4.23
27	TTK	NM_003318	-4.77	77	CEP55	NM_018131	-4.21
28	PKMYT1	NM_182687	-4.76	78	CASC5	NM_170589	-4.20
29	CIT	NM_007174	-4.71	79	CCNB2	NM_004701	-4.20
30	BUB1	NM_004336	-4.71	80	HIST2H3A	NM_001005464	-4.20
31	CENPM	NM_001002876	-4.70	81	HJURP	NM_018410	-4.20
32	GTSE1	NM_016426	-4.70	82	CKS2	NM_001827	-4.19
33	C9orf140	NM_178448	-4.67	83	DEPDC1B	NM_018369	-4.19
34	DLGAP5	NM_014750	-4.66	84	NUSAP1	NM_016359	-4.13
35	CENPF	NM_016343	-4.66	85	TSPAN8	NM_004616	-4.13
36	CEP55	NM_018131	-4.64	86	NEK2	NM_002497	-4.11
37	PBK	NM_018492	-4.62	87	NCEH1	NM_020792	-4.10
38	VAMP3	NM_004781	-4.61	88	TAF9B	NM_015975	-4.08
39	AURKB	NM_004217	-4.60	89	KIF20B	NM_016195	-4.07
40	ATAD2	NM_014109	-4.59	90	KIF23	NM_138555	-4.06
41	TFRC	NM_003234	-4.58	91	ADAMTS1	NM_006988	-4.05
42	TNFRSF6B	NM_003823	-4.58	92	MLF1IP	NM_024629	-4.01
43	TPX2	NM_012112	-4.58	93	HIST1H1B	NM_005322	-3.99
44	KIF4A	NM_012310	-4.57	94	BCL2A1	NM_004049	-3.97
45	KIF11	NM_004523	-4.57	95	ST6GALNAC1	NM_018414	-3.92
46	DIAPH3	NM_001042517	-4.54	96	CCL23	NM_005064	-3.92
47	RN5-8S1	NR_003285	-4.53	97	RFK	NM_018339	-3.87
48	APOBEC3B	NM_004900	-4.53	98	BRIP1	NM_032043	-3.82
49	NDC80	NM_006101	-4.51	99	HSD11B1	NM_181755	-3.72
50	BIRC5	NM_001012271	-4.51	100	HIST1H3B	NM_003537	-3.35

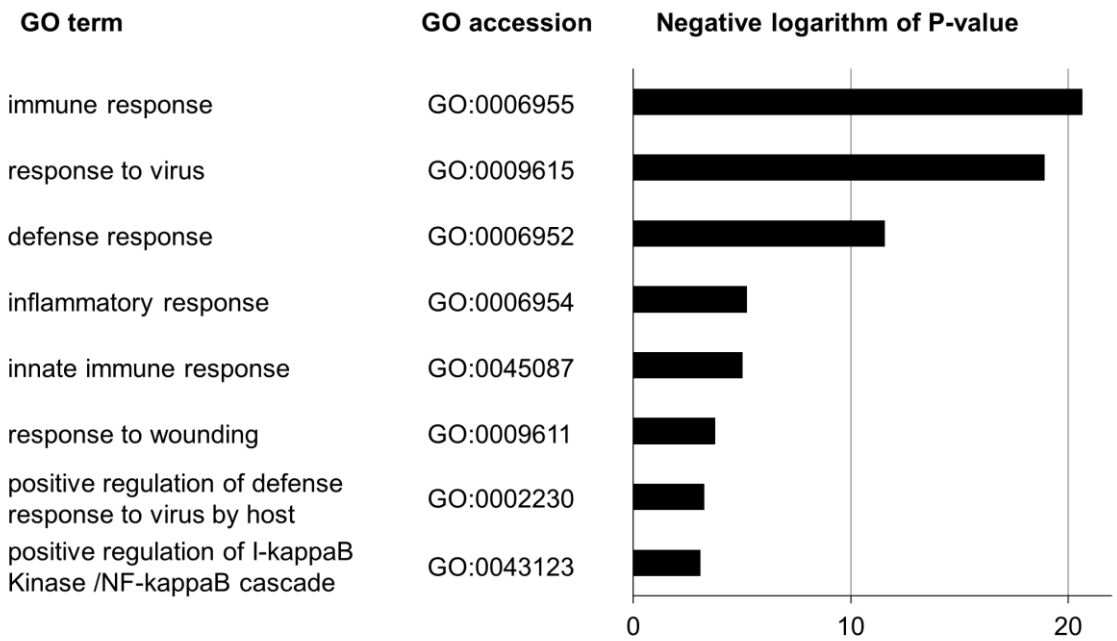

Supplementary Fig. S1 | Negative logarithm of P-value for enrichment of the functional category in gene ontology (GO). The corresponding GO terms and accession codes are listed on the left.

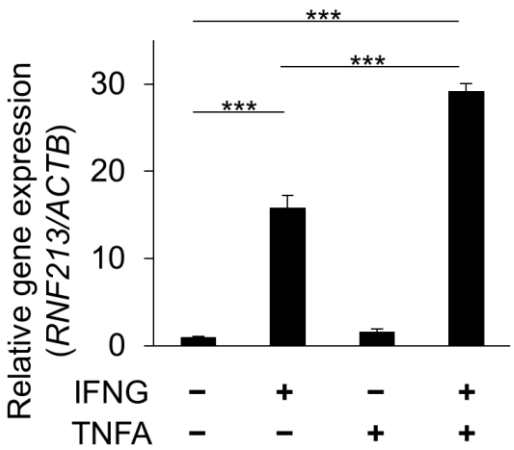

Supplementary Fig. S2 | Synergistic effects of IFNG and TNFA on transcriptional activation of *RNF213* in HCAECs. Relative expression levels of *RNF213* in the presence (+) or absence (-) of IFNG and TNFA are shown as mean ± SD values (n = 3). *ACTB* was used as internal control. ***$p < 0.001$.

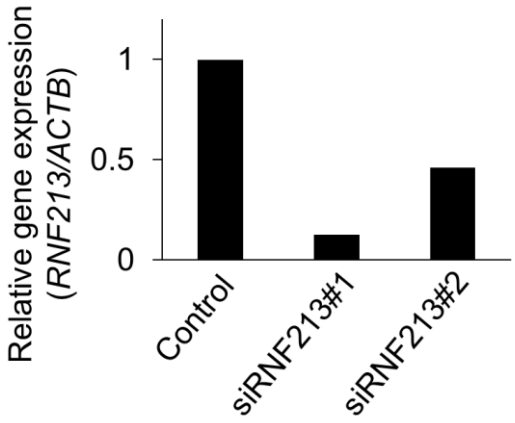

Supplementary Fig. S3 | *In vitro* knockdown of *RNF213* with synthetic siRNA duplexes in HCAECs. Data represent the mean values of relative expression of *RNF213* at 48 hr after treatment of HCAECs with indicated siRNAs. Error bars were omitted because data with >95% of accuracy was obtained in two independent assays.

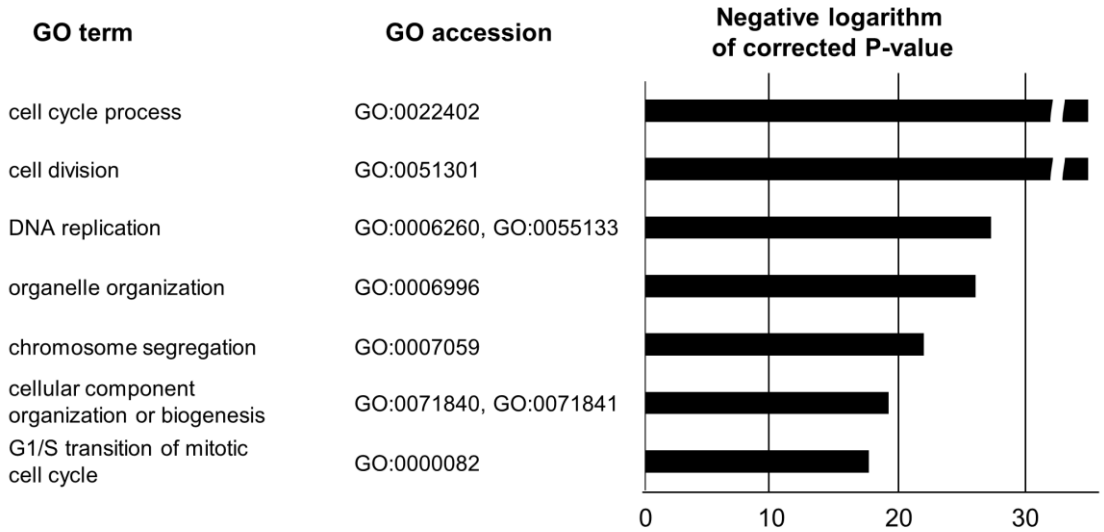

Supplementary Fig. S4 | Negative logarithm of corrected P-value for enrichment of the functional category in gene ontology (GO). The corresponding GO terms and accession codes are listed on the left.

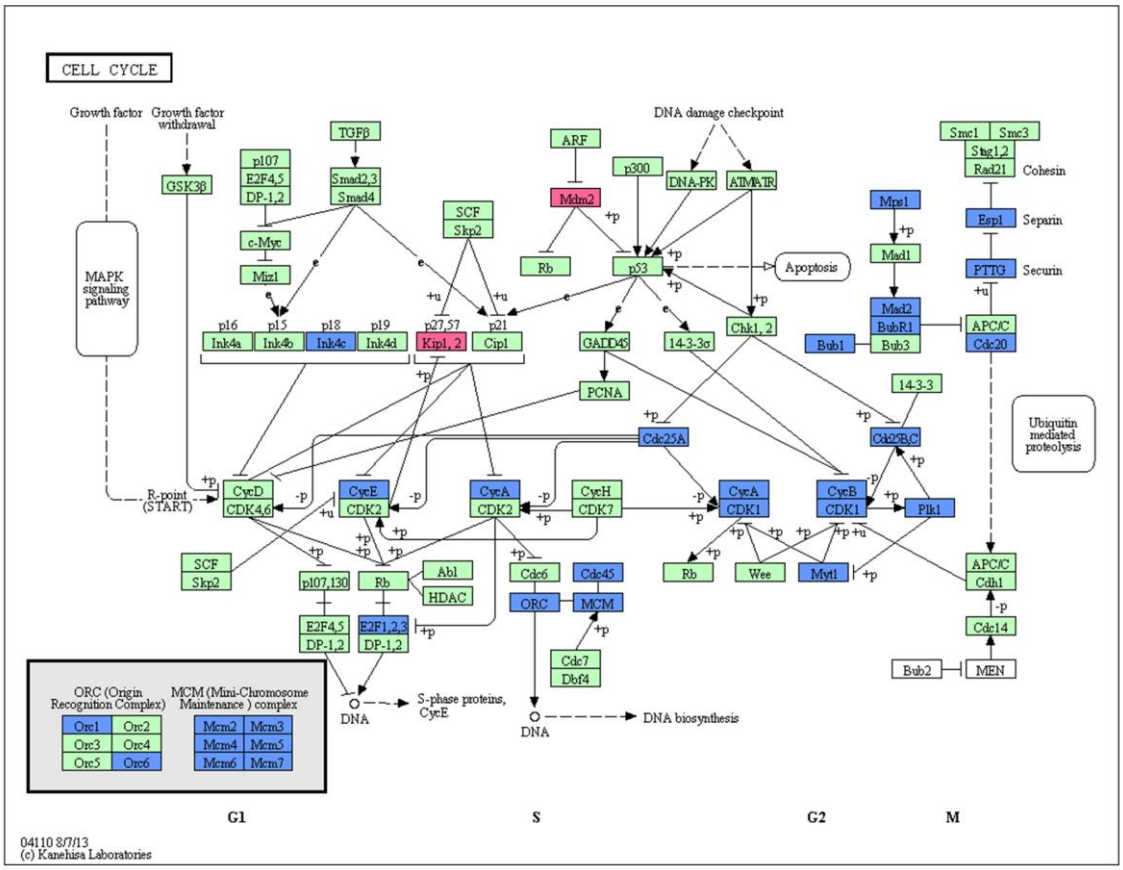

Supplementary Fig. S5 | KEGG pathway analysis for the transcriptome data with siRNA-mediated knockdown of *RNF213* in endothelial cells. The color codes indicate up-regulated (red), down-regulated (blue) and other genes (green).

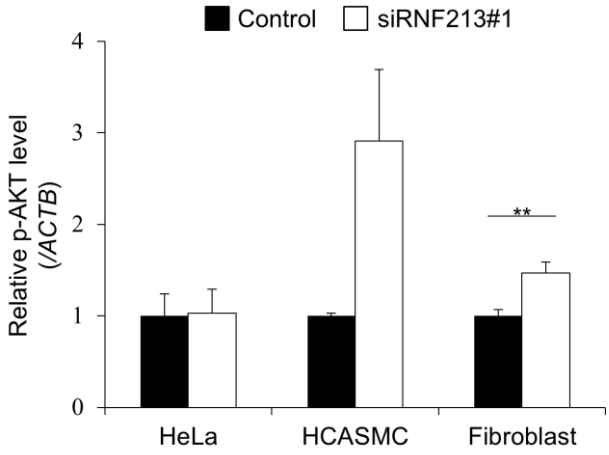

Supplementary Fig. S6 | Western blots for p-AKT level for HeLa, HCASMCs or fibroblasts. SiRNA-mediated knockdown of *RNF213* (siRNF213#1) did not decrease p-AKT level in those cells (n = 3 in each group). "Control" represents the cells treated with control siRNA. Data are shown as mean ± SD values and analyzed using Student's t-test. **p < 0.01.

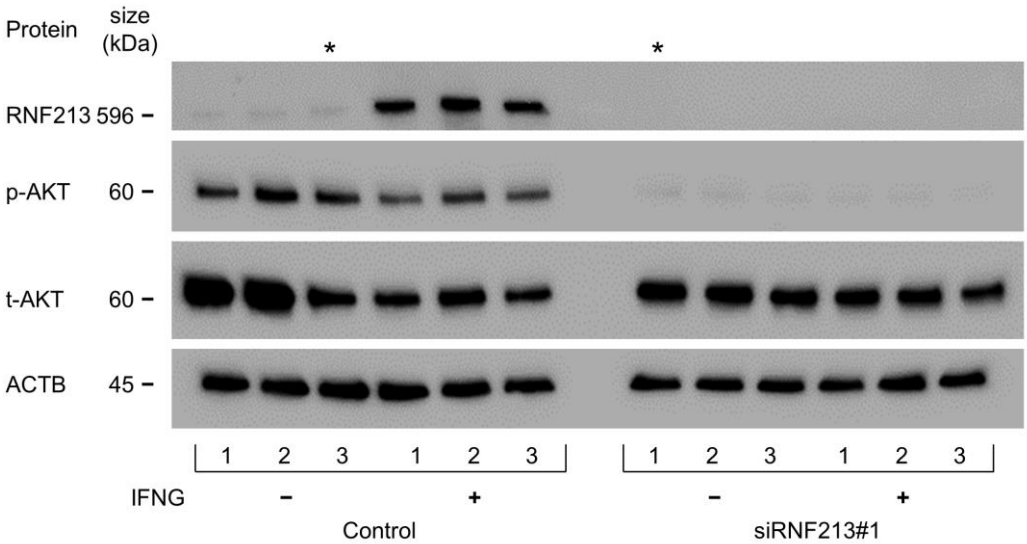

Supplementary Fig. S7 | The original western blot images in HUVECs. The immuno-probed proteins and the molecular size are indicated on the left. The footnotes annotate the conditions of IFNG and the siRNA treatments in triplicate (1-3). Asterisks indicate the two lanes selected for **Fig. 3e**.

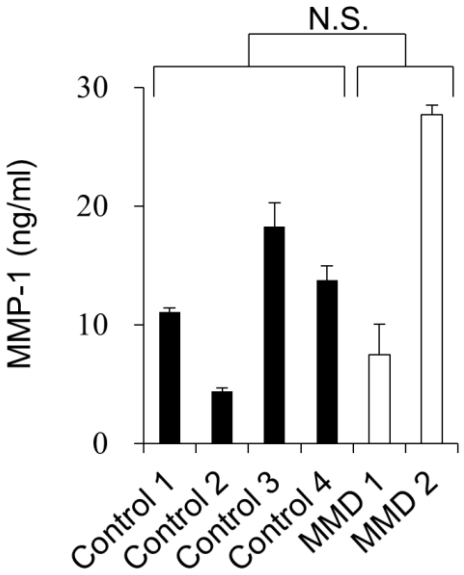

Supplementary Fig. S8 | MMP1 protein levels at basal condition in fibroblasts from 4 healthy controls and 2 MMD patients. Data are shown as mean ± SD values (n = 3) and analyzed using Student's t-test. N.S., not significant.

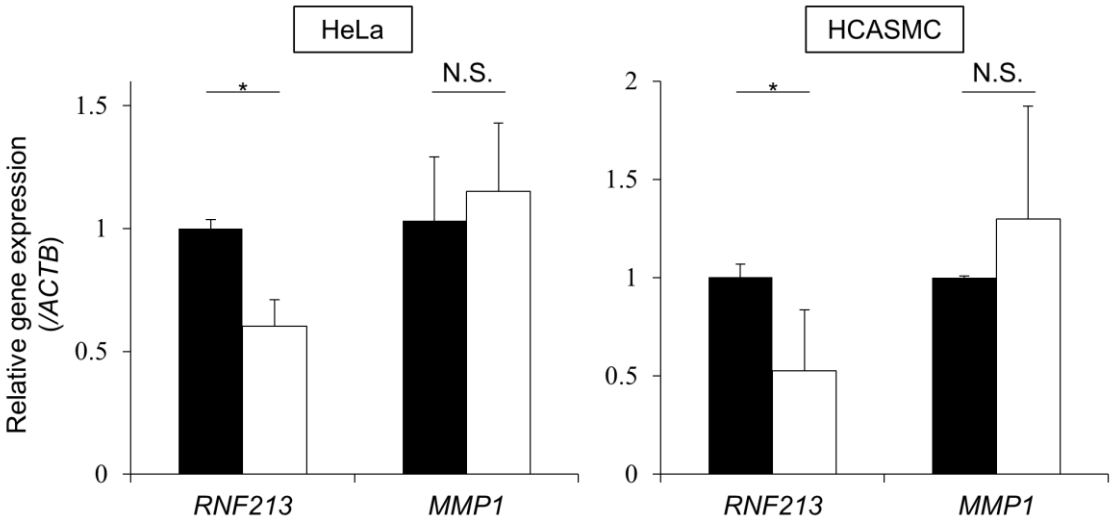

Supplementary Fig. S9 | Negligible effects of the *RNF213* silencing on *MMP1* expression in HeLa and HCASMAs cells. Plots are shown as mean ± SD (n = 3) and analyzed using Student's t-test. *p < 0.05. N.S., not significant.

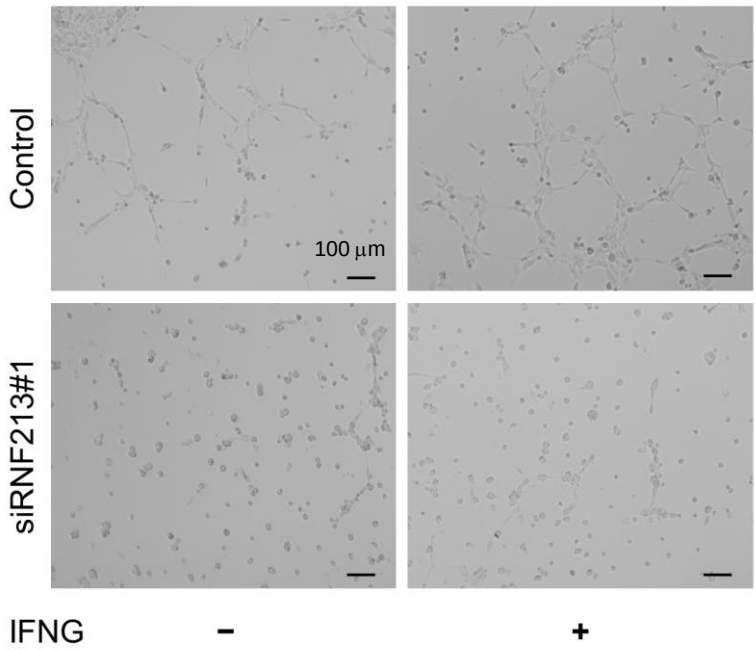

Supplementary Fig. S10 | The angiogenic responses of HCAECs on matrigels in different conditions. Representative images for tubular formation by trypsinized HCAECs in the absence (upper panels) or the presence of siRNA for *RNF213* (lower). Effects of IFNG pretreatments (right) on angiogenic response of HCAECs are shown in comparison with those of untreated cells (left). Scale bar = 100 μm.

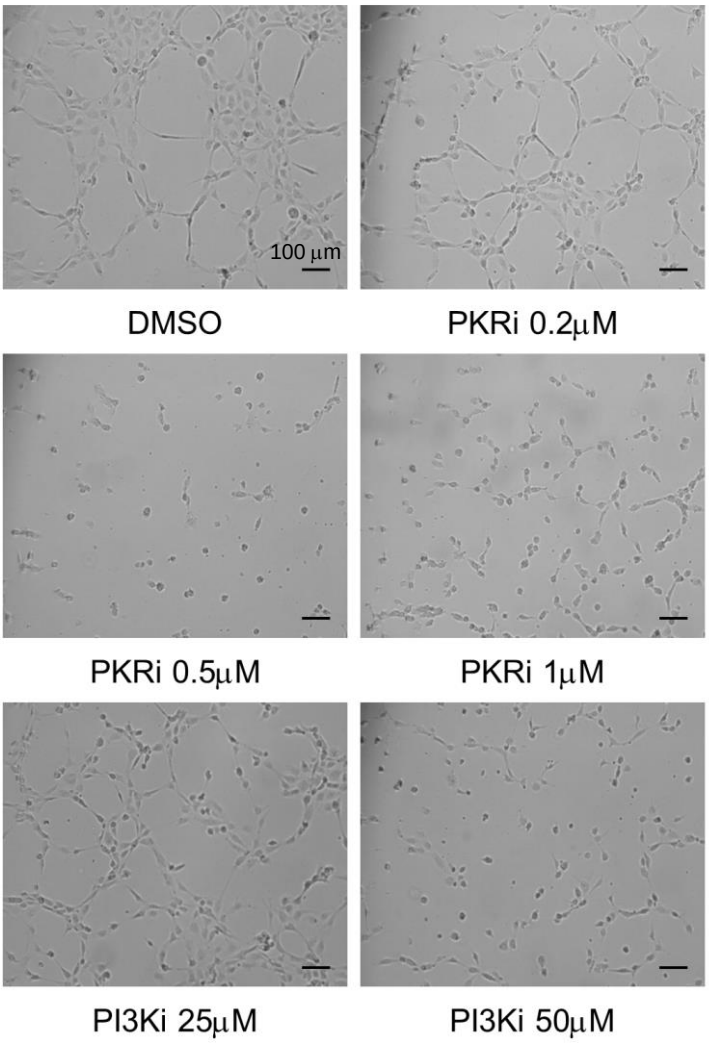

Supplementary Fig. S11 | PI3K and PKR inhibitors disrupt the tubular formations of HUVECs on the matrigel. The images of growing HUVECs on matrigels were captured at 4 hr after inoculation. Applied compounds (DMSO, LY294002 and C16) are annotated at the bottom of each panel. Scale bar = 100 μm.

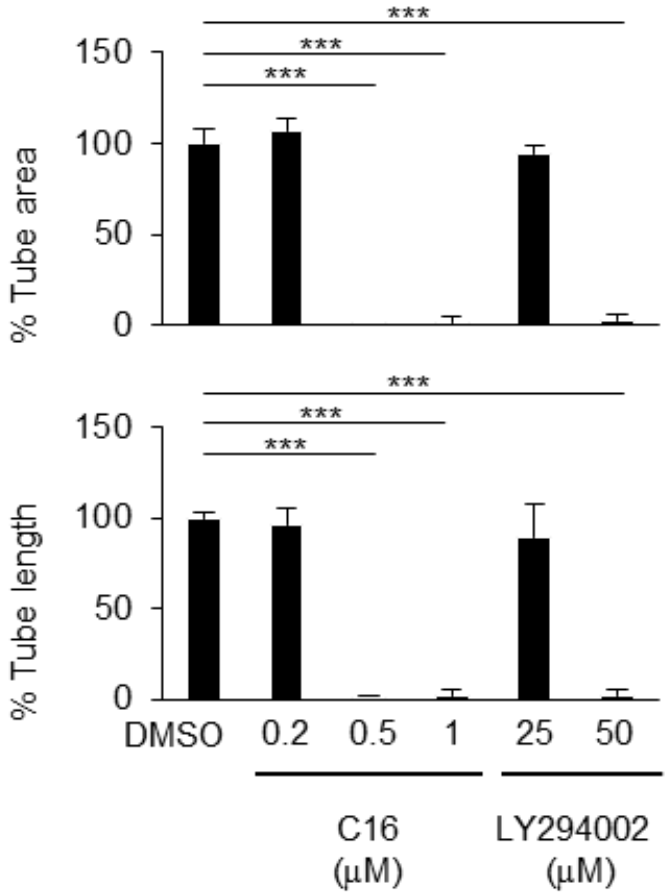

Supplementary Fig. S12 | The quantitative data for Supplementary Fig. S11. % tube area (upper) and length (lower) are shown as mean ± SD plots (n = 3) and analyzed using Dunnett's test. ***$p < 0.001$.